

## Chapter XX: Ultrafast optical parametric amplifiers

*Giulio Cerullo and Sandro De Silvestri*

Dipartimento di Fisica, Politecnico

Piazza L. da Vinci 32, 20133 Milano, Italy

### 1. Introduction

Many applications of ultrafast optics require femtosecond pulses with not only short duration, but also broad frequency tunability. As an example, in pump-probe experiments [1] both pump and probe pulses need to be frequency tunable, in order to excite a system on resonance and probe optical transitions occurring at different photon energies. Ti:sapphire lasers with Kerr-lens mode-locking [2] and chirped-pulse amplification (CPA) [3] are now widely used sources of stable, energetic femtosecond pulses. Typical figures of commercial Ti:sapphire laser systems are pulse energy  $>1$  mJ, pulse duration  $<100$  fs and repetition rate  $>1$  kHz. However the frequency tunability of such laser sources is limited in a narrow range around the fundamental wavelength (FW) of  $0.8$   $\mu\text{m}$  or around the second harmonic (SH) of  $0.4$   $\mu\text{m}$ . Despite this limitation, the very high peak powers of these systems, in excess of  $10$  GW, enable exploiting the second order nonlinear optical effect known as Optical Parametric Generation (OPG) to extend their tuning range.

The principle of OPG is quite simple [4-8]: in a suitable nonlinear crystal, an high frequency and high intensity beam (the *pump* beam, at frequency  $\omega_p$ ) amplifies a lower frequency, lower intensity beam (the *signal* beam, at frequency  $\omega_s$ ); in addition a third beam (the *idler* beam, at frequency  $\omega_i$ ) is generated. In the OPG process, signal and idler beams play an interchangeable role. Throughout this chapter we assume that the signal is at higher frequency, i.e.  $\omega_s > \omega_i$ . The OPG process can be given a simple corpuscular interpretation: a photon at frequency  $\omega_p$  is absorbed by a virtual level of the material and two photons at frequencies  $\omega_s$  and  $\omega_i$  are emitted. In this interaction both energy conservation

$$\hbar\omega_p = \hbar\omega_i + \hbar\omega_s \quad (1)$$

and momentum conservation

$$\hbar k_p = \hbar k_i + \hbar k_s \quad (2)$$

must be fulfilled. The signal frequency to be amplified can vary in principle from  $\omega_p/2$  (the so-called degeneracy condition) to  $\omega_p$ , and correspondingly the idler varies from  $\omega_p/2$  to 0; at degeneracy, signal and idler have the same frequency. In summary, the OPG process transfers energy from a high-power, fixed frequency pump beam to a low-power, variable frequency signal beam; in this process a third beam, the idler, is also generated. The OPG process thus provides a broadband optical amplifier with continuously tunable center frequency; to be efficient, it requires very high intensities of the order of tens of  $\text{GW}/\text{cm}^2$  and is therefore eminently suited to femtosecond laser systems, which can easily achieve such intensities even with modest energies, of the order of a few  $\mu\text{J}$ .

OPG can be exploited in two ways to achieve frequency tunability: if the OPG crystal is enclosed in a suitable optical cavity and the parametric gain exceeds the losses, the cavity starts oscillating like an ordinary laser and an optical parametric oscillator (OPO) is obtained. A completely different approach consists in amplifying a suitably generated weak signal beam (the so-called “seed” beam) in one or more OPG crystals, thus obtaining an optical parametric amplifier (OPA). Both schemes are employed with ultrashort pulses, as well as in cw and ns-pulse systems, and each has its advantages and drawbacks. OPOs can be pumped by a small-scale femtosecond oscillator, and provide pulses at very high repetition rates ( $\approx 100$  MHz). This helps in ultrafast spectroscopy experiments detecting very weak signals to improve signal-to-noise ratio [9-12]. On the other hand, OPO output energies are low (typically a few nJs), and they require a cavity whose length is matched to that of the pump laser to within micrometers, calling for active cavity length stabilization. Their tunability is limited by the bandwidth of the mirror coatings, so that several mirror sets may be needed to span the whole tuning range; replacement of a mirror set is not trivial,

since it requires to align the OPO cavity and simultaneously match its length with that of the pump oscillator to guarantee synchronous pumping. OPAs require high pump intensities, provided only by an amplified system, and operate at lower repetition rates (typically from 1 to 100 kHz); on the other hand, they provide high output energies, broad frequency tunability and are simpler to operate, since they do not require any cavity length stabilization. Therefore femtosecond OPOs and OPAs are complementary systems, used in different types of applications; however, OPAs are gaining increasing popularity due to their simplicity and ease of operation.

In this chapter we will focus on femtosecond OPAs, starting from the basic concepts and covering also the most recent developments [13]. In Section 2 we will briefly review some basic concepts of second-order nonlinear optics; in Section 3 we present the theory of optical parametric amplification for monochromatic waves; in section 4 we point out the main issues arising with ultrashort pulses, deriving some design criteria. In section 5 we introduce the basic architecture of a femtosecond OPA; in section 6 we present some classical designs of femtosecond OPA systems, covering the near-IR, visible and mid-IR spectral ranges. In section 7 we show how OPAs have the capability of generating pulses much shorter than the pump pulses, exploiting the ultrabroad gain bandwidths available in certain configurations. In section 8 we will describe another unique feature of OPAs, namely the capability to generate, under suitable conditions, pulses with a constant carrier-envelope phase. Finally in section 9 we will show how OPAs, thanks to their very high gain and low thermal loading, may provide an alternative route to the generation of ultrahigh peak power pulses, exceeding the PW level.

## 2. *Second order nonlinear optics.*

Let us consider an electromagnetic wave crossing a material; the time-varying electric field induces in the atoms/molecules a time-dependent polarization, which in turn drives light emission. At low intensities, the polarization is a linear function of the electric field

$$P_L(t) = \epsilon_0 \chi^{(1)} E(t) \quad (1)$$

where  $\varepsilon_0$  is the free-space permittivity and  $\chi^{(l)}$  is the linear dielectric susceptibility. As the intensity increases, further nonlinear terms in which the polarization is proportional to higher powers of the electric field must be considered

$$P(t) = \varepsilon_0 \left[ \chi^{(1)} E(t) + \chi^{(2)} E^2(t) + \chi^{(3)} E^3(t) + \dots \right] \quad (2)$$

where  $\chi^{(2)}$  and  $\chi^{(3)}$  are the second and third order nonlinear susceptibilities. Symmetry arguments can be used to show that the even orders of susceptibility are zero in isotropic materials. The polarization can then be divided in a linear and a non-linear part:  $P(t) = P_L(t) + P_{NL}(t)$ . If we now limit ourselves to second order terms (and thus to propagation in anisotropic bulk materials), we get

$$P_{NL}(z, t) = \varepsilon_0 d_{eff} E^2(z, t) \quad (3)$$

where  $d_{eff}$  is the so-called effective non-linear optical coefficient, which is linked through the tensor  $\chi^{(2)}$  to the propagation direction and polarisation of the field. Let us now consider the superposition of two monochromatic plane waves at frequencies  $\omega_1$  and  $\omega_2$  (with  $\omega_1 < \omega_2$ ) propagating in the medium:

$$E(z, t) = \frac{1}{2} A_1(z, t) \exp[j(\omega_1 t - k_1 z)] + \frac{1}{2} A_2(z, t) \exp[j(\omega_2 t - k_2 z)] + c.c. \quad (4)$$

The nonlinear polarization becomes

$$P_{NL}(z, t) = \frac{\varepsilon_0 d_{eff}}{4} \left\{ \begin{array}{l} 2|A_1|^2 + 2|A_2|^2 + A_1^2 \exp j(2\omega_1 t - 2k_1 z) + A_2^2 \exp j(2\omega_2 t - 2k_2 z) + \\ 2A_1 A_2 \exp j[(\omega_1 + \omega_2)t - (k_1 + k_2)z] + \\ 2A_1^* A_2 \exp j[(\omega_2 - \omega_1)t - (k_2 - k_1)z] + c.c. \end{array} \right\} \quad (5)$$

The various terms of this equation describe a wealth of nonlinear optical phenomena. The non-oscillating terms correspond to **optical rectification**, the terms at  $2\omega_1$  and  $2\omega_2$  to **second harmonic generation** (SHG), that at  $\omega_1 + \omega_2$  to **sum-frequency generation** (SFG) and that at  $\omega_2 - \omega_1$  to **difference-frequency generation** (DFG). Let us examine these last two phenomena in greater detail.

In SFG (Fig. 1a) two fields at frequencies  $\omega_1$  and  $\omega_2$  interact to produce a field at the frequency  $\omega_3 = \omega_1 + \omega_2$  (SHG is just a particular case in which  $\omega_1 = \omega_2$ ). In terms of photons balance, two photons at energies  $\hbar\omega_1$  and  $\hbar\omega_2$  are absorbed to a virtual level of the material, and a sum-frequency photon with energy  $\hbar\omega_3 = \hbar\omega_1 + \hbar\omega_2$  is emitted. In DFG (Fig. 1b) two fields at frequencies  $\omega_1$  and  $\omega_2$  interact; the field at  $\omega_2$  loses energy in favour of the field at  $\omega_1$  and of the newly generated frequency  $\omega_3 = \omega_2 - \omega_1$  (optical rectification is the limiting case when  $\omega_1 = \omega_2$ ). In terms of photon balance, a photon with energy  $\hbar\omega_2$  is absorbed to a virtual level of the material, and a photon at energy  $\hbar\omega_1$  stimulates the emission of a second photon at the same energy, in addition to a photon at the energy  $\hbar\omega_3$  to complete the decay to the ground state.

OPG is a mechanism similar to DFG, except for the strength of the interacting fields: DFG arises when the fields at  $\omega_1$  and  $\omega_2$  have comparable intensities, while OPG occurs when the field at  $\omega_1$  is much weaker. In OPG, therefore, an intense beam at  $\omega_p$  (*pump* beam) transfers energy to the beam at  $\omega_s$  (*signal* beam), thereby amplifying it, and generates a beam at the difference frequency  $\omega_i$  (*idler* beam).

### 3. Theory of optical parametric amplification.

In this paragraph we briefly review the theory of optical parametric amplification [7, 8]. We start with a linearly polarized light pulse with carrier frequency  $\omega$ , envelope  $A(z,t)$  and plane wavefront, propagating in the  $z$  direction

$$E(z,t) = \frac{1}{2} A(z,t) \exp[j(\omega t - kz)] + c.c. \quad (6)$$

in a medium with a second order non-linear polarisation. According to Maxwell's equations, the propagation of the field in the nonlinear material can be described by the

$$\frac{\partial^2 E(z,t)}{\partial z^2} - \mu_0 \frac{\partial^2 D(z,t)}{\partial t^2} = \mu_0 \frac{\partial^2 P_{NL}(z,t)}{\partial t^2} \quad (7)$$

where  $D$  is the electric displacement field due to the linear polarization in the material and  $\mu_0$  is the magnetic permeability of vacuum. Upon inserting Eq. (6) into (7) and assuming the *Slowing Varying Envelope Approximation* (SVEA), i.e. variations of  $A$  that are small over propagation distances of the order of the wavelength ( $\left| \frac{\partial^2 A}{\partial z^2} \right| \ll \left| 2k \frac{\partial A}{\partial z} \right|$ ), and considering linear dispersion, one

gets [8]

$$-2jk \left[ \frac{\partial A}{\partial z} + \frac{\partial k}{\partial \omega} \frac{\partial A}{\partial t} + \frac{1}{2j} \frac{\partial^2 k}{\partial \omega^2} \frac{\partial^2 A}{\partial t^2} \right] \exp[j(\omega t - kz)] = \mu_0 \frac{\partial^2 P_{NL}(z, t)}{\partial t^2} \quad (8)$$

By defining the group velocity  $v_g = \frac{\partial \omega}{\partial k}$  and the group velocity dispersion (GVD)  $D = \frac{\partial^2 k}{\partial \omega^2}$ , Eq.

(8) can be recast in the form:

$$-2jk \left[ \frac{\partial A}{\partial z} + \frac{1}{v_g} \frac{\partial A}{\partial t} + \frac{1}{2j} D \frac{\partial^2 A}{\partial t^2} \right] \exp[j(\omega t - kz)] = \mu_0 \frac{\partial^2 P_{NL}(z, t)}{\partial t^2} \quad (9)$$

This equation shows that the pulse envelope propagates through the medium with the group velocity  $v_g$ , while GVD causes a change of its shape; the nonlinear polarization acts as a source term driving its amplitude and frequency variations.

Let us now consider the propagation in a second order nonlinear medium of three collinear linearly polarized quasi-monochromatic waves at frequencies  $\omega_i$ ,  $\omega_s$  and  $\omega_p$ , with  $\omega_i < \omega_s < \omega_p$  and  $\omega_i + \omega_s = \omega_p$ . The polarizations of the three waves are not necessarily parallel. The resulting electric field can be written as:

$$E(z, t) = \frac{1}{2} \left\{ \begin{aligned} &A_i(z, t) \exp[j(\omega_i t - k_i z)] + A_s(z, t) \exp[j(\omega_s t - k_s z)] + \\ &A_p(z, t) \exp[j(\omega_p t - k_p z)] + c.c. \end{aligned} \right\} \quad (10)$$

If we assume that only the interaction  $\omega_i + \omega_s = \omega_p$  is phase-matched (see Par. 3.1), then the only relevant terms in the nonlinear second order polarization are

$$\begin{aligned}
P_{NL}(z, t) = & 2\varepsilon_0 d_{eff} A_s^*(z, t) A_p(z, t) \exp j[\omega_i t - (k_p - k_s)z] + \\
& + 2\varepsilon_0 d_{eff} A_i^*(z, t) A_p(z, t) \exp j[\omega_s t - (k_p - k_i)z] + \\
& + 2\varepsilon_0 d_{eff} A_i(z, t) A_s(z, t) \exp j[\omega_p t - (k_i + k_s)z] + c.c.
\end{aligned} \tag{11}$$

Eq. (11) shows that: (i) the nonlinear polarisation at one frequency is proportional to the product of the electric fields at the other two frequencies, so that the waves become nonlinearly coupled; (ii) the wavevector of the nonlinear polarization at a given frequency  $\omega_j$  does not coincide with that of the wave,  $k_j$ .

The forcing term  $\partial^2 P_{NL} / \partial t^2$  can be easily calculated and simplified applying the SVEA, thus getting:

$$\begin{aligned}
\frac{\partial^2 P_{NL}}{\partial t^2} = & -2\varepsilon_0 d_{eff} \omega_i^2 A_s^*(z, t) A_p(z, t) \exp j[\omega_i t - (k_p - k_s)z] + \\
& - 2\varepsilon_0 d_{eff} \omega_s^2 A_i^*(z, t) A_p(z, t) \exp j[\omega_s t - (k_p - k_i)z] + \\
& - 2\varepsilon_0 d_{eff} \omega_p^2 A_i(z, t) A_s(z, t) \exp j[\omega_p t - (k_i + k_s)z] + c.c.
\end{aligned} \tag{12}$$

By inserting (12) into (9) and rejecting the complex conjugated, one derives the three coupled non-linear equations:

$$\frac{\partial A_i}{\partial z} + \frac{1}{v_{gi}} \frac{\partial A_i}{\partial t} + \frac{1}{2j} D_i \frac{\partial^2 A_i}{\partial t^2} = -\frac{j d_{eff} \omega_i}{c_0 n_i} A_s^* A_p \exp[-j\Delta k z] \tag{13a}$$

$$\frac{\partial A_s}{\partial z} + \frac{1}{v_{gs}} \frac{\partial A_s}{\partial t} + \frac{1}{2j} D_s \frac{\partial^2 A_s}{\partial t^2} = -\frac{j d_{eff} \omega_s}{c_0 n_s} A_i^* A_p \exp[-j\Delta k z] \tag{13b}$$

$$\frac{\partial A_p}{\partial z} + \frac{1}{v_{gp}} \frac{\partial A_p}{\partial t} + \frac{1}{2j} D_p \frac{\partial^2 A_p}{\partial t^2} = -\frac{j d_{eff} \omega_p}{c_0 n_p} A_i A_s \exp[j\Delta k z] \tag{13c}$$

where  $\Delta k = k_p - k_s - k_i$  is the so-called wave vector mismatch. Eqs. (13) show that the three fields exchange energy through the nonlinear polarization: if two fields are injected into the medium, a third one is generated by the non-linear interaction.

Let us first simplify Eqs. (13) by considering monochromatic waves, so that  $\frac{\partial A(z,t)}{\partial t} = 0$  and

$\frac{\partial^2 A(z,t)}{\partial t^2} = 0$ . We get:

$$\frac{\partial A_i}{\partial z} = -\frac{jd_{eff}\omega_i}{c_0 n_i} A_s * A_p \exp(-j\Delta kz) \quad (14a)$$

$$\frac{\partial A_s}{\partial z} = -\frac{jd_{eff}\omega_s}{c_0 n_s} A_i * A_p \exp(-j\Delta kz) \quad (14b)$$

$$\frac{\partial A_p}{\partial z} = -\frac{jd_{eff}\omega_p}{c_0 n_p} A_i A_s \exp(j\Delta kz) \quad (14c)$$

These equations can be easily solved if one neglects the depletion of the pump beam ( $A_p \cong \text{const.}$ ) and assumes an initial signal intensity  $A_{s0}$  (seed beam) and no initial idler beam ( $A_{i0} = 0$ ). In this case one has two coupled linear equations linking the signal and idler beams. For the signal one gets:

$$\frac{\partial^2 A_s}{\partial z^2} = -j\Delta k \frac{\partial A_s}{\partial z} + \Gamma^2 A_s \quad (15)$$

where:  $\Gamma^2 = \frac{2d_{eff}^2 \omega_i \omega_s}{c_0^3 \epsilon_0 n_i n_s n_p} I_p$  and the beam intensity is calculated as:  $I_j = \frac{1}{2} n_j c \epsilon_0 |A_j|^2$ .

One obtains, after propagation for a length  $L$  of nonlinear material:

$$I_s(L) = I_{s0} \left\{ 1 + \left[ \frac{\Gamma}{g} \sinh(gL) \right]^2 \right\} \quad (16a)$$

$$I_i(L) = I_{s0} \frac{\omega_i}{\omega_s} \left[ \frac{\Gamma}{g} \sinh(gL) \right]^2 \quad (16b)$$

where:

$$g = \sqrt{\Gamma^2 - \left( \frac{\Delta k}{2} \right)^2} \quad (17)$$

In the case of large gain ( $gL \gg 1$ ), Eqs. (16) simplify to

$$I_s(L) = \frac{1}{4} \left( \frac{\Gamma}{g} \right)^2 I_{s0} \exp(2gL) \quad (18a)$$

$$I_i(L) = \frac{\omega_i}{4\omega_s} \left( \frac{\Gamma}{g} \right)^2 I_{s0} \exp(2gL) \quad (18b)$$

When  $\Delta k = 0$ ,  $g = \Gamma$  and expressions (18) further simplify into:

$$I_s(L) = \frac{1}{4} I_{s0} \exp(2gL) \quad (19a)$$

$$I_i(L) = I_{s0} \frac{\omega_i}{\omega_s} \exp(2gL) \quad (19b)$$

Eqs. (18) and (19) show that, for a given small-signal gain, both signal and idler intensities grow exponentially (within the no-depletion approximation) with crystal length  $L$  and allow to define a parametric gain as

$$G = \frac{I_s(L)}{I_{s0}} = \frac{1}{4} \left( \frac{\Gamma}{g} \right)^2 \exp(2gL) \quad (20)$$

Note that this exponential growth is qualitatively different from the quadratic growth observed in other second-order processes like SFG and SHG and shows that the OPA behaves like a real amplifier. With respect to a classical optical amplifier based on population inversion in an atomic or molecular transition, however, an OPA has three important differences;

- (i) it does not have any energy storage capability, i.e. the gain is present only during the pump pulse;
- (ii) the gain center frequency is not fixed, but can be continuously adjusted by varying the phase matching condition;
- (iii) the gain bandwidth is not limited by the linewidth of the transition, but rather by the possibility of satisfying the phase matching condition over a broad range of frequencies.

Let us now consider the factors influencing the parametric gain  $G$ :

1)  $G \propto \exp(g)$  exponentially depends on the parameter  $g$ , which is maximum when  $\Delta k = 0$  (phase-matching condition).  $G$  rapidly decreases for non-zero values of  $\Delta k$ , suggesting that phase-matching is a key condition to be fulfilled in order to get significant amplification from the non-linear material. In the following we will focus on the case  $\Delta k = 0$ , leading to  $g = \Gamma$ .

2)  $G \propto \exp(d_{eff})$  depends exponentially on the second order nonlinear optical coefficient of the crystal  $d_{eff}$ ; one should therefore select the crystal with the highest  $d_{eff}$ . There are however other considerations leading to the choice of the crystal, such as phase matching range, dispersive properties, availability and optical damage threshold.

3)  $G \propto \exp(\sqrt{I_p})$  scales as the exponential of the square root of the pump intensity. This indicates the suitability of ultrashort pulses for OPAs, due to their high peak powers. One should try to use the highest possible pump intensity before the onset of other nonlinear optical phenomena such as self-focusing, self-phase modulation and beam breakup. In order to be able to use high pump intensities, it is important to have a spatially clean beam profile, without hot spots.

4)  $G \propto \exp(L)$  scales as the exponential of the crystal length. This dependence is strikingly different from that of SHG efficiency, which scales as the square of the crystal length. This difference can be understood intuitively in the following way: in a strong pump field, the presence of a seed photon at the signal wavelength stimulates the generation of an additional signal photon and of a photon at the idler wavelength. Likewise, due to the symmetry of signal and idler, the amplification of an idler photon stimulates the generation of a signal photon. Therefore, the generation of the signal field reinforces the generation of the idler field and vice versa, giving rise to a positive feedback that is responsible for the exponential growth of the waves. We will see that with ultra-short light pulses the optimum crystal length has to be chosen considering the durations and group velocities of the interacting pulses.

5)  $G \propto \exp(\sqrt{\omega_i \omega_s})$  scales as the exponential of the square root of the product of signal and idler frequencies. This seems to indicate an advantage to use high pump frequencies. However we

will see that with ultrashort pulses this advantage is often offset by the larger difference in group velocities of the interacting pulses.

In the following we discuss some examples of parametric gain calculation relevant to ultrashort pulses, assuming perfect phase matching. Fig.2(a) shows a plot of the parametric gain in BBO, at the infrared pump wavelength  $\lambda_p = 0.8 \mu\text{m}$  and the signal wavelength  $\lambda_s = 1.2 \mu\text{m}$ , as a function of pump intensity and for different crystal lengths. At a pump intensity  $I_p = 25 \text{ GW/cm}^2$ , a gain  $G \cong 6$  is calculated for a crystal length  $L = 1 \text{ mm}$ ; however it rapidly increases to  $G \cong 2 \times 10^6$  for  $L = 5 \text{ mm}$ . The same gain can be obtained with a 3-mm crystal increasing the pump intensity to  $75 \text{ GW/cm}^2$ . The same plot for BBO at the visible pump wavelength  $\lambda_p = 0.4 \mu\text{m}$  and the signal wavelength  $\lambda_s = 0.6 \mu\text{m}$  is shown in Fig. 2. In this case, at a pump intensity  $I_p = 25 \text{ GW/cm}^2$ , a gain  $G \cong 128$  is calculated for a crystal length  $L = 1 \text{ mm}$ , about a factor of 20 larger than in the case of infrared pump. The higher gain is due to the larger values of  $\omega_s$  and  $\omega_i$ , which increase the parametric gain. Despite this improvement, the group velocity mismatch between the interacting pulses, as we will see later, prevents the use of long nonlinear crystals in this case.

### 3.1 Energy and momentum conservation.

Let us first discuss the energy balance in the OPA process. By taking the derivative of the intensity of each wave with respect to the propagation direction

$$\frac{\partial I_j}{\partial z} = \frac{1}{2} n_j c_0 \epsilon_0 \left( \frac{\partial A_j}{\partial z} A_j^* + A_j \frac{\partial A_j^*}{\partial z} \right) \quad (21)$$

and inserting Eqs. (14) in (21), one gets the equations

$$\frac{\partial I_i}{\partial z} = -\frac{1}{2} j d_{eff} \epsilon_0 \omega_i \left( A_i^* A_s^* A_p e^{-j\Delta kz} - A_i A_s A_p^* e^{j\Delta kz} \right) \quad (22a)$$

$$\frac{\partial I_s}{\partial z} = -\frac{1}{2} j d_{eff} \epsilon_0 \omega_s \left( A_i^* A_s^* A_p e^{-j\Delta kz} - A_i A_s A_p^* e^{j\Delta kz} \right) \quad (22b)$$

$$\frac{\partial I_p}{\partial z} = \frac{1}{2} j d_{eff} \epsilon_0 \omega_p \left( A_i^* A_s^* A_p e^{-j\Delta k z} - A_i A_s A_p^* e^{j\Delta k z} \right) \quad (22c)$$

which can be cast into the form

$$\frac{1}{\omega_i} \frac{\partial I_i}{\partial z} = \frac{1}{\omega_s} \frac{\partial I_s}{\partial z} = - \frac{1}{\omega_p} \frac{\partial I_p}{\partial z} \quad (23)$$

Eqs. (23), also known as Manley-Rowe relations, state energy conservation in the parametric interaction. In fact, by defining a photon flux  $\Phi = \frac{I}{\hbar\omega}$  as the number of photons incident on the unitary surface per unit of time, Eq. (23) can be rewritten as

$$\frac{d\Phi_i}{dz} = \frac{d\Phi_s}{dz} = - \frac{d\Phi_p}{dz} \quad (24)$$

Eqs. (24) are consistent with the corpuscular interpretation of the OPA process: for each photon at  $\omega_p$  absorbed by the virtual level, one photon at  $\omega_i$  and one at  $\omega_s$  are simultaneously emitted.

Let us now discuss the phase-matching condition  $\Delta k = 0$ , which is required for an efficient OPA process. To get a physical insight into its meaning, we can consider that, at each position inside the nonlinear optical material, new frequency components are generated locally, driven by the nonlinear optical polarization, and then propagate with their own phase velocity. In order to get a macroscopic effect all the generated components must add up in phase at the exit of the material. This is possible

only if their phase velocity is equal to that of the forcing term,  $\frac{\partial^2 P_{NL}}{\partial t^2}$ . Let us consider for example

the process of DFG/OPG:  $\omega_i = \omega_p - \omega_s$ . In this case the difference frequency wave propagates with

the phase velocity  $v_{Pi} = \frac{\omega_i}{k_i}$ , while the nonlinear polarization driving the process has the phase

velocity  $v_{PNL} = \frac{\omega_i}{k_p - k_s}$ , so that they propagate with the same velocity only when  $\Delta k = 0$ .

Let us now discuss how to obtain the collinear phase-matching condition  $\Delta k = 0$  necessary for high gain. The condition  $k_p = k_i + k_s$  is equivalent to

$$n_p = \frac{\omega_i n_i + \omega_s n_s}{\omega_p} \quad (25)$$

It is easy to show that (25) is normally not satisfied in isotropic materials; in the limiting case  $\omega_i = \omega_s = \omega$ ,  $\omega_p = 2\omega$  (SHG), it would correspond to  $n(2\omega) = n(\omega)$ , which is not possible because of normal dispersion. More generally, assuming  $n_i < n_s < n_p$ , we can show that Eq. (25) can be rewritten as

$$\omega_p (n_p - n_s) = \omega_i (n_i - n_s) \quad (26)$$

which cannot be satisfied since the two sides have opposite sign. This shows that phase matching is not obtainable in isotropic media with normal dispersion. In birefringent crystals, which are anyway those used for OPAs because, due to the lack of inversion symmetry, they have a second order nonlinear optical coefficient, one can exploit the polarization dependence of refractive index. In particular, one can choose for the high frequency pump field the polarization direction corresponding to the lower refractive index. One can then select the propagation direction in the crystal in order to exactly satisfy (25) for a given set of wavelengths.

We consider the case, common in femtosecond OPAs, of negative uniaxial birefringent crystals ( $n_e < n_o$ ); according to the previous discussion, the pump beam has extraordinary polarization. If both signal and idler beam have ordinary polarization, we talk about type I phase matching. If either the signal or the idler beams have extraordinary polarization, we talk about type II phase matching [14]. Both types of phase matching have their specific advantages and can be used depending on the case. Usually the phase matching condition is achieved by adjusting the angle  $\theta_m$  between the wave vector of the propagating beams and the optical axis of the nonlinear crystal (angular phase matching). Alternatively, the refractive indexes can be changed by varying the crystal temperature (temperature phase matching).

As an example, let us consider type I phase matching in a negative uniaxial crystal (such as for example BBO). In this case Eq. (25) becomes:

$$n_{ep}^* = \frac{\omega_i n_{oi} + \omega_s n_{os}}{\omega_p} \quad (27)$$

which allows to compute  $n_{ep}^*$ , i.e. the refractive index at the pump frequency required for phase matching. The refractive index of the extraordinary beam depends on the angle  $\theta$  between the wave vector and the optical axis according to the:

$$\frac{1}{n_e^2(\theta)} = \frac{\sin^2(\theta)}{n_e^2} + \frac{\cos^2(\theta)}{n_o^2} \quad (28)$$

where  $n_e$  is the principal extraordinary refractive index. Putting together (27) and (28) one obtains the phase matching angle as

$$\theta_m = \arcsen \left[ \frac{n_{ep}}{n_{ep}^*} \sqrt{\frac{n_{op}^2 - n_{ep}^{*2}}{n_{op}^2 - n_{ep}^2}} \right] \quad (29)$$

In this case the idler is efficiently generated with ordinary polarisation, while extraordinary components are negligible since phase-mismatched. For type II phase matching, equation (27) cannot be solved explicitly, only approximate solutions can be found with numerical methods [14]. Figure 3 shows the phase matching angle as a function of wavelength for BBO type I and II OPAs at 0.8  $\mu\text{m}$  pump wavelength. Note that, in general, the phase matching angle has a less pronounced wavelength dependence for type I with respect to type II phase matching.

#### 4. Parametric amplification with ultrashort pulses: group-velocity mismatch, gain bandwidth.

So far we have discussed the case of monochromatic waves ( $\partial A(z, t) / \partial t = 0$ ); we will now see how the previous considerations can be extended to ultrashort OPAs. In this case one needs to go back to Eqs. (13), containing the time derivatives of the pulse envelopes. As previously discussed, the second derivatives describe broadening of the individual pulses within the nonlinear crystal due to

dispersion, and can be neglected for the pulsewidths and propagation lengths normally used in OPAs. By transforming to a frame of reference that is moving with the group velocity of the pump pulse ( $\tau = t - z/v_{gp}$ ) we obtain the equations

$$\frac{\partial A_i}{\partial z} + \left( \frac{1}{v_{gi}} - \frac{1}{v_{gp}} \right) \frac{\partial A_i}{\partial \tau} = - \frac{j d_{eff} \omega_i}{c_0 n_i} A_s * A_p \exp[-j \Delta k z] \quad (30a)$$

$$\frac{\partial A_s}{\partial z} + \left( \frac{1}{v_{gs}} - \frac{1}{v_{gp}} \right) \frac{\partial A_s}{\partial \tau} = - \frac{j d_{eff} \omega_s}{c_0 n_s} A_i * A_p \exp[-j \Delta k z] \quad (30b)$$

$$\frac{\partial A_p}{\partial z} = - \frac{j d_{eff} \omega_p}{c_0 n_p} A_i A_s \exp[j \Delta k z] \quad (30c)$$

These equations show that the main limiting factor in parametric interaction with ultrashort pulses is the difference in group velocities, also called group velocity mismatch (GVM), between the interacting pulses. With respect to the pump pulse, which is fixed in this frame of reference, the signal and idler pulses move with different velocities and after a while separate temporally, thus stopping the parametric interaction. The relative speeds  $v_{grel}$  of signal and idler pulses with respect to the pump pulse are given, according to (30), by

$$\frac{1}{v_{grel j}} = \frac{1}{v_{gj}} - \frac{1}{v_{gp}} \quad j = i, s \quad (31)$$

Given a pump pulse with duration  $\tau$ , one can define pulse splitting length as the propagation length after which the signal (or the idler) pulse temporally separates from the pump pulse in the absence of gain; this represents the length over which parametric interaction takes place, i.e. the maximum useful crystal length. It can be expressed as

$$l_{jp} = \tau v_{grel j} \quad j = i, s \quad (32)$$

Note that the pulse splitting length becomes shorter for decreasing pulse duration and for increasing GVM. GVM depends on the crystal type, pump wavelength and type of phase matching. Figs. 4 and 5 show examples of GVM curves for a BBO OPA pumped at 0.8  $\mu\text{m}$  (Fig. 4) and 0.4  $\mu\text{m}$  (Fig.

5), respectively. Note that, due to greater dispersion values in the visible, GVM is in general larger in this wavelength range.

We have shown that the GVM between pump and signal/idler limits the maximum useful length of the nonlinear crystal. We will now consider which factors determine the amplification bandwidth. Ideally one would like to have a broadband amplifier, i.e. an amplifier which, for a fixed pump frequency  $\omega_p$ , provides a more or less constant gain over a broad range of signal frequencies. In order to achieve broadband amplification, one needs to keep the phase mismatch  $\Delta k$  as small as possible over a large bandwidth. Practically, however, the phase matching condition can be satisfied only for a given set of frequencies  $(\tilde{\omega}_i, \tilde{\omega}_s, \tilde{\omega}_p)$ , so that

$$\Delta k = k(\tilde{\omega}_p) - k(\tilde{\omega}_s) - k(\tilde{\omega}_i) = 0 \quad (33)$$

If the pump frequency is fixed at  $\tilde{\omega}_p$  and the signal frequency changes to  $\tilde{\omega}_s + \Delta\omega$ , then by energy conservation the idler frequency changes to  $\tilde{\omega}_i - \Delta\omega$ . The ensuing wave vector mismatch becomes

$$\Delta k = k(\tilde{\omega}_p) - [k(\tilde{\omega}_s) + \Delta k_s] - [k(\tilde{\omega}_i) + \Delta k_i] = -\Delta k_i - \Delta k_s \quad (34)$$

which can be approximated to the first order as

$$\Delta k \cong -\frac{\partial k_s}{\partial \omega_s} \Delta\omega + \frac{\partial k_i}{\partial \omega_i} \Delta\omega = \left( \frac{1}{v_{gi}} - \frac{1}{v_{gs}} \right) \Delta\omega \quad (35)$$

The full width at half maximum parametric gain bandwidth can then be calculated from Eq. (20), within the large gain and low pump-depletion approximations, as:

$$\Delta\nu = \frac{2(\ln 2)^{1/2}}{\pi} \left( \frac{\Gamma}{L} \right)^{1/2} \frac{1}{\left| \frac{1}{v_{gi}} - \frac{1}{v_{gs}} \right|} \quad (36)$$

Eq. (36) shows that the gain bandwidth is inversely proportional to the GVM between signal and idler and has only a square root dependence on small-signal gain and crystal length. For the case when  $v_{gi} = v_{gs}$ , Eq. (36) loses validity and (35) must be expanded to the second order, giving

$$\Delta\nu = \frac{2(\ln 2)^{1/4}}{\pi} \left(\frac{\Gamma}{L}\right)^{1/4} \frac{1}{|D_i + D_s|} \quad (37)$$

Figures 6 and 7 show typical plots of phase matching bandwidths for BBO OPAs, pumped at 0.8  $\mu\text{m}$  (Fig. 6) and 0.4  $\mu\text{m}$  (Fig. 7), respectively. We see a remarkable difference between type I and II phase matching: for type II interaction, the bandwidth is smaller than in type I and stays more or less constant over the tuning range, while for type I interaction, as previously said, the bandwidth increases as the OPA approaches degeneracy. These features can be exploited for different applications: type I phase matching is used to achieve the shortest pulses, while type II phase matching allows to obtain relatively narrow bandwidths over broad tuning ranges, which are required for many spectroscopic investigations.

### 5. General architecture of an ultrafast OPA

A general scheme of an ultrafast OPA is presented in Fig. 8. The system is powered by energetic femtosecond pulses, typically coming from an amplified Ti:sapphire laser at 800 nm. A fraction of the beam is split and used to generate the seed beam. Then the pump beam (which may be optionally frequency doubled) and the seed, after their timing has been adjusted by a delay line, interact in a first amplification stage. It is possible to further amplify the signal in a second stage (power amplifier), using a previously split fraction of the pump beam. The two-stage approach has two advantages: (i) it allows to compensate from the GVM arising between pump and signal beams in the first stage; (ii) it enables to adjust the pump intensity, and thus the parametric gain, separately in the two stages. In particular the power amplifier requires a much lower gain. At the OPA output, after the pump has been spectrally filtered, both signal and idler beams are available. In some cases, it may be necessary to use a pulse compressor to restore the transform-limited (TL) duration of the pulses.

#### 5.1 Seed pulse generation

The first stage of any OPA is the seed generator, i.e. a stage producing the initial photons at the signal wavelength. Since the seed beam is at a different wavelength than the pump beam, a nonlinear process is required for its production. The two main techniques employed for seed generation are parametric superfluorescence and supercontinuum generation.

Parametric superfluorescence [15] is parametric amplification of vacuum noise and can also be thought as two-photon emission from a virtual level excited by the pump field. In practice it is achieved by pumping a suitable second order nonlinear crystal (often of the same kind as those employed in the later OPA stages); amplification of vacuum noise occurs at those wavelengths for which the phase-matching condition is satisfied. Disadvantages of this technique are the poor spatial quality of the generated seed beam and its large fluctuations (inherent in a process which is starting from noise); for these reasons, it is nowadays seldom used in OPAs.

Supercontinuum (white light) generation [16] is a phenomenon occurring when an intense light pulse is focused inside a transparent material, such as fused silica or sapphire. It can be understood as a result of self-phase-modulation (SPM) of the pulse. When an intense laser beam impinges on a material of thickness  $L$ , its refractive index becomes a linear function of the intensity (Kerr effect):

$$n(t) = n_0 + n_2 I(t) \quad (38)$$

so that the phase shift experienced by a quasi-monochromatic pulse of carrier frequency  $\omega_0$  is

$$\phi(t) = \omega_0 t - \frac{\omega_0}{c_0} n(t) L = \omega_0 t - \frac{\omega_0}{c_0} n_0 L - \frac{\omega_0}{c_0} n_2 L I(t) \quad (39)$$

and the instantaneous frequency becomes

$$\omega(t) = \frac{d\phi(t)}{dt} = \omega_0 - \frac{\omega_0 n_2 L}{c_0} \frac{dI}{dt} = \omega_0 \left( 1 - \frac{n_2 L}{c_0} \frac{dI}{dt} \right). \quad (40)$$

Eq. (40) suggests that the instantaneous carrier frequency of the pulse changes in time; in particular, during the leading edge of the pulse ( $dI/dt > 0$ ) it is shifted to the red, while during the trailing edge ( $dI/dt < 0$ ) it is shifted to the blue, leading to a dramatic broadening of the spectrum. Note that this

is an oversimplified description of the phenomenon: in fact other phenomena such as spatial self-focusing, temporal self-steepening and space time-focusing play a role (see [17] and [18] for a detailed description).

Practically, white light generation is typically achieved by focusing 800-nm, 100-fs pulses with energy from 1 to 3  $\mu\text{J}$  into a sapphire plate, with thickness ranging between 1 and 3 mm. Sapphire is chosen because of excellent thermal conductivity and low UV absorption, preventing long-term degradation. The white light extends throughout the visible (down to  $\approx 0.4 \mu\text{m}$ ) and the near-IR (up to  $\approx 1.5 \mu\text{m}$ ), with an energy of approximately 10 pJ per nm of bandwidth; it displays very high pulse-to-pulse stability and excellent spatial beam quality.

## 6. *OPAs from the visible to the mid-IR*

In this section we present several standard OPA designs over different frequency ranges.

### 6.1 *OPAs in the near-IR*

The simplest way of obtaining OPAs tunable in the near-IR is by pumping with the fundamental wavelength (800 nm) of an amplified Ti:sapphire laser [19-26]. In this case we have the following advantages:

- (i) high available pump energies (up to the mJ-level);
- (ii) low pump-signal and pump-idler GVM values, allowing the use of long nonlinear crystals and the obtainment of high gains.

These advantages are partially offset by a lower gain for the parametric interaction in the near-IR compared to the visible because of lower signal and idler frequencies. Tunability is limited by the losses due to absorption of the idler wave in the nonlinear crystal. This is typically a problem at wavelengths longer than  $\approx 3 \mu\text{m}$ . Therefore the signal beam is tunable from degeneracy (1.6  $\mu\text{m}$ ) to 1.1  $\mu\text{m}$  while the idler beam tunes from 1.6 to 3  $\mu\text{m}$ . This leaves a “hole” in the tuning range from 0.8 to 1.1  $\mu\text{m}$ .

A typical setup for a near-IR OPA is shown in Fig. 9 [27]: it is pumped by a standard CPA Ti:sapphire laser generating 500- $\mu\text{J}$ , 50-fs pulses at 1 kHz repetition rate. A small fraction of the pump ( $\approx 2 \mu\text{J}$ ) is used to generate white light in a 2-mm-thick sapphire plate. 50  $\mu\text{J}$  of the pump are used to amplify a near-IR wavelength in the continuum in a preamplifier stage consisting of a 3-mm-thick BBO crystal cut for type II phase matching ( $\theta = 26^\circ$ ,  $\varphi = 0^\circ$ ). Wavelength tuning is achieved by tilting the crystal, thus changing the phase matching condition. Typical signal energies after the preamplifier are up to 6  $\mu\text{J}$ . The power amplifier stage consists of an identical BBO crystal pumped by 450  $\mu\text{J}$ ; in this case amplified pulse energies up to 200  $\mu\text{J}$  are generated. The signal beam is tunable from 1.1 to 1.6  $\mu\text{m}$  and the idler up to 2.8  $\mu\text{m}$ ; pulsewidth ranges from 30 to 50 fs according to wavelength.

### *6.2 OPAs in the visible*

A straightforward way of achieving tunable visible pulses consists in frequency doubling the output of an 800-nm-pumped near-IR OPA [26]; however, since absorption of the idler in the nonlinear crystal prevents signal amplification for wavelengths shorter than  $\approx 1100 \text{ nm}$ , the SH would be tunable down to only 550 nm, leaving a substantial part of the visible range uncovered. Pumping with the SH of an amplified Ti:sapphire laser around 400 nm [28-33], the signal can be tuned through most of the visible range, from  $\approx 450 \text{ nm}$  to degeneracy (800 nm). Correspondingly, the idler tunes from 800 nm to 3  $\mu\text{m}$ ; this fills the gap in the tuning range left by near-IR OPAs. Visible OPAs in general produce lower energies than near-IR ones, because of the lower pump energy available from a frequency doubled pump. Furthermore GVM is much larger in the visible range, preventing the use of long nonlinear crystals. This disadvantage is partially compensated for by the larger gain for parametric interaction in the visible. Also in visible OPAs the most popular nonlinear material is BBO. Type II phase matching provides gain bandwidths that are narrower and stay essentially constant over the tuning range, which may be beneficial for some spectroscopic

applications [30]. Using type I phase matching, the amplified pulse bandwidth strongly depends on signal wavelength, increasing in the red as degeneracy is approached. The collinear interaction geometry limits the available phase matching bandwidth. A solution to this problem, which consists in using a non-collinear interaction geometry, will be discussed in Section 7, in which also the experimental details of the visible OPA will be given.

### *6.3 OPAs in the mid-IR*

The mid-IR spectral region (3-10  $\mu\text{m}$ ) is spectroscopically very interesting because it covers the vibrational transitions in molecules and the intersubband transitions in low-dimensional semiconductors. The most widely used approach for the generation of tunable mid-IR pulses is based on DFG between signal and idler pulses generated by a near-IR OPA pumped at 800 nm [34-36]. A typical experimental setup is shown in Fig. 10: the signal and idler pulses are generated by a type II near-IR OPA, and thus have perpendicular polarization, as required in the DFG process. The two pulses, with a combined energy of  $\approx 200 \mu\text{J}$ , are separated by a dichroic mirror, reflecting the idler and transmitting the signal, and recombined by an identical mirror: in this way their relative delay can be adjusted. The two collinear and temporally overlapped pulses are then focused on a 1-mm-thick  $\text{AgGaS}_2$  crystal, cut for type II phase-matching ( $\theta = 40^\circ$ ); the mid-IR pulses are separated from the residual near-IR by a long-pass filter and collimated by an off-axis paraboloid. By tuning the OPA and simultaneously readjusting the phase matching angle of the DFG crystal, the mid-IR pulses can be tuned from 3 to 10  $\mu\text{m}$  with energies in excess of 1  $\mu\text{J}$ ; pulsewidths down to 70 fs, corresponding to just a few cycles of the mid-IR electric field, are obtained.

## *7. Non-collinear OPAs for ultrabroadband visible pulse generation*

OPAs provide an easy way of tuning over a broad range the frequency of an otherwise fixed femtosecond laser system, and this is their main spectroscopic application. On the other hand they

can be broadband optical amplifiers and thus can be used to dramatically shorten, by more than an order of magnitude, the duration of the pump pulse. One can therefore start with a femtosecond system producing relatively long pulses (100-200 fs) and use an OPA to shorten their duration to the sub-10-fs regime. In this Section we will describe such ultrabroadband OPAs based on non-collinear phase matching.

We have seen in Section 4 that the gain bandwidth of an OPA is determined by the GVM between signal and idler pulses. In an OPA using a collinear interaction geometry, the propagation direction in the nonlinear crystal is selected to satisfy, for a given signal wavelength, the phase-matching condition  $\Delta k = 0$ . In this configuration the signal and idler group velocities are fixed and so the phase matching bandwidth of the process (see Eq. 36). An additional degree of freedom can be introduced using a non-collinear geometry, such as that shown in Fig. 11(a): pump and signal wave-vectors form an angle  $\alpha$  (independent of signal wavelength) and the idler is emitted at an angle  $\Omega$  with respect to the signal. In this case the phase matching condition is a vector equation, which, projected on directions parallel and perpendicular to the signal wave-vector, becomes

$$\Delta k_{par} = k_p \cos \alpha - k_s - k_i \cos \Omega = 0 \quad (41a)$$

$$\Delta k_{perp} = k_p \sin \alpha - k_i \sin \Omega = 0 \quad (41b)$$

Note that the angle  $\Omega$  is not fixed, but depends on the signal frequency. If the signal frequency increases by  $\Delta\omega$ , the idler frequency decreases by  $\Delta\omega$  and the wave-vector mismatches along the two directions can be approximated, to the first order, as

$$\Delta k_{par} \cong -\frac{\partial k_s}{\partial \omega_s} \Delta\omega + \frac{\partial k_i}{\partial \omega_i} \cos \Omega \Delta\omega - k_i \sin \Omega \frac{\partial \Omega}{\partial \omega_i} \Delta\omega \quad (42a)$$

$$\Delta k_{perp} \cong \frac{\partial k_i}{\partial \omega_i} \sin \Omega \Delta\omega + k_i \cos \Omega \frac{\partial \Omega}{\partial \omega_i} \Delta\omega \quad (42b)$$

To achieve broadband phase matching, both  $\Delta k_{par}$  and  $\Delta k_{perp}$  must vanish. Upon multiplying (42a) by  $\cos \Omega$  and (42b) by  $\sin \Omega$  and adding the results, we get

$$\frac{\partial k_i}{\partial \omega_i} - \cos \Omega \frac{\partial k_s}{\partial \omega_s} = 0 \quad (43)$$

which is equivalent to

$$v_{gs} = v_{gi} \cos \Omega. \quad (44)$$

Eq. (44) shows that broadband phase-matching can be achieved for a signal-idler angle  $\Omega$  such that the signal group velocity equals the projection of the idler group velocity along the signal direction. This effect is shown pictorially in Fig. 11: for a collinear geometry (Fig. 11(b)), signal and idler moving with different group velocities get quickly separated giving rise to pulse lengthening and bandwidth reduction, while in the non-collinear case (Fig. 11(c)) the two pulses manage to stay effectively overlapped. Note that Eq. (44) can be satisfied only if  $v_{gi} > v_{gs}$ ; this is however always the case in the commonly used type I phase matching in negative uniaxial crystals, where both signal and idler see the ordinary refractive index. Eq. (44) allows to determine the signal-idler angle  $\Omega$  required for broadband phase-matching; from a practical point of view, it is more useful to know the pump-signal angle  $\alpha$ , which is given by

$$\alpha = \arcsin \left( \frac{1 - v_{gs}^2 / v_{gi}^2}{1 + 2v_{gs}n_s\omega_s / v_{gi}n_i\omega_i + n_s^2\omega_s^2 / n_i^2\omega_i^2} \right)^{1/2} \quad (45)$$

Note that in a practical situation the pump-signal angle  $\alpha$  is determined by the propagation direction of the seed beam, while the signal idler angle  $\Omega$  adjusts itself, according to (41b), to satisfy the phase matching condition: so the idler is emitted at a different angle for each wavelength, i.e. is angularly dispersed.

As an example, in a type I BBO OPA pumped at 400 nm, for a signal wavelength of 600 nm broadband non-collinear phase-matching is achieved, according to (45), for  $\alpha = 3.7^\circ$ . To better illustrate the effect of non-collinear phase-matching, in Fig. 12 we plot, for the above described OPA, the phase matching angle  $\theta_m$  as a function of signal wavelength for different values of  $\alpha$ . For a collinear configuration ( $\alpha = 0^\circ$ )  $\theta_m$  shows a strong dependence on the signal wavelength so that, for a

fixed crystal orientation, phase-matching can be achieved only over a narrow signal frequency range. By going to a non-collinear configuration and increasing  $\alpha$ , the wavelength dependence of  $\theta_m$  becomes progressively weaker until, for the optimum value  $\alpha = 3.7^\circ$ , a single crystal orientation ( $\theta \cong 31^\circ$ ) allows to achieve simultaneously phase matching over an ultra-broad bandwidth, extending from 0.5 to 0.75  $\mu\text{m}$ .

This favourable property of the non-collinear geometry for broadband parametric amplification, first recognized by Gale *et al.* [37, 38], is exploited to build the non-collinear OPA (NOPA) [39-45].

In the following we will describe a typical NOPA design [40, 42, 44], the schematic of which is shown in Fig. 13. The system starts with a conventional CPA Ti:sapphire laser generating 150-fs, 800-nm pulses at 1 kHz with energy up to 500  $\mu\text{J}$ . The system has enough energy for simultaneously pumping up to three NOPAs. A fraction of the beam is used to generate the pump pulses at 400 nm by SHG in a 1-mm-thick lithium triborate crystal; they have energy up to 50  $\mu\text{J}$  and their duration is slightly lengthened to  $\approx 180$  fs by GVM during the SHG process. Another small fraction of the beam, with energy of approximately 2  $\mu\text{J}$ , is focused into a 1-mm-thick sapphire plate to generate the seed pulses; by carefully controlling the energy incident on the plate (using a variable-optical-density attenuator) and the position of the plate around the focus, a highly stable single-filament white light continuum is generated. The group delay of the visible portion of the white light, measured with the technique of optical Kerr gating, is small and fairly linear with frequency, with group-delay dispersion (GDD) ranging from 75  $\text{fs}^2$  at 700 nm to 115  $\text{fs}^2$  at 500 nm; the measured chirp matches fairly well the GDD introduced by the sapphire plate. This can be understood by recalling that, as explained in Sect. 5.1, most of the visible frequency components are generated in a short time interval during the leading edge of the pulse, around the point of maximum steepness. To avoid the introduction of additional chirp, only reflective optics are employed to guide the white light to the amplification stage. Parametric gain is achieved in a 1-mm-

thick BBO crystal, cut at  $\theta = 31^\circ$ , using a single-pass configuration to increase the gain bandwidth. The chosen crystal length is close to the pulse-splitting length for signal and pump in the wavelength range of interest. To minimize the effects of self-focusing, we position the BBO crystal beyond the focus of the pump beam. In that position the pump spot size is approximately  $120 \mu\text{m}$ , corresponding to an intensity of  $120 \text{ GW}/\text{cm}^2$ ; at higher intensities distortions and beam breakup are observed. The white-light seed is imaged by a spherical mirror (Fig. 13) in the BBO crystal, with a spot size matching that of the pump beam.

When it is illuminated by the pump pulse and aligned perpendicularly to the pump beam, the BBO crystal emits a strong off-axis parametric superfluorescence in the visible in a cone with an apex angle of  $6.15^\circ$  (corresponding to an angle of  $3.7^\circ$  inside the crystal); this is the direction for which the group velocities of signal and idler are matched and therefore the gain bandwidth is maximized. We carefully adjust the pump-signal angle to match the cone apex angle, giving us a visual aid in order to optimise the system for broadband phase-matching. In these conditions, for optimum pump–seed delay, an ultrabroad gain bandwidth that extends over most of the visible is observed. A typical amplified pulse spectrum shown in Fig. 14(a): It displays a FWHM of  $180 \text{ THz}$ . The amplified pulses have energy of approximately  $2 \mu\text{J}$ , peak-to-peak fluctuations of less than 2% and maintain a good  $\text{TEM}_{00}$  beam quality. Higher energies, up to  $\approx 10 \mu\text{J}$ , can be extracted by a second pass in the BBO crystal. After the gain stage the amplified pulses are collimated by a spherical mirror and sent to the compressor.

The NOPA generates pulses with very broad bandwidths and thus potentially very short: in order to obtain the minimum pulsewidth compatible with their bandwidth (the so-called TL duration), one needs to accurately control their spectral phase. The NOPA pulses have a positive chirp due to material propagation; simple compressors can be obtained by double-passing prism pairs or grating pairs. This correction is sufficient for pulses with moderately broad bandwidths, since TOD cannot be controlled independently. For ultrabroadband pulses one can use prism-grating sequences in

order to be able to correct simultaneously second and third order dispersion [43, 46]; alternatively, one can use compressors with custom-tailored dispersion characteristics, which can accurately correct to high orders the phase distortions in the system. Such compressors are either chirped dielectric mirrors, in which both GDD and TOD can be independently controlled, or adaptive systems based on deformable mirrors. Using ultrabroadband double-chirped mirrors, pulses as short as 5.7 fs have been generated from NOPAs [44, 47], while the pulsewidth could be pushed down to 3.9 fs using deformable mirrors [45, 48].

While some applications benefit from the ultrabroad bandwidths generated by the visible NOPA under optimum alignment, in other cases it is necessary to be more frequency selective and reduce the NOPA bandwidth, generating pulses which are still very short (15-20 fs) but have center frequencies tunable across the visible range. Two possible strategies to reach this goal are: (i) increasing the chirp of the white light before the amplification stage; (ii) detuning the pump-signal angle  $\alpha$  from the optimum value. In the first case the spectral components of the white light seed are properly delayed so that only few components are temporally overlapped to the 180-fs-pump and get amplified. This can be easily obtained by adding a glass block on the seed path; its thickness changes the group delay of the various colours and influences the bandwidth of the seed superposed to and amplified by the pump. Tunability, on the contrary, is obtained adjusting the seed-pump delay only, thanks to the broad acceptance bandwidth of the amplifying crystal. The disadvantage of this technique lays in the need to compensate for the chirp added by the glass, which increases when thicker glasses are chosen.

In order to avoid any correction in the compression stage, a second approach can be adopted: since, as already explained through Fig. 12, the amplified bandwidth depends on the angle  $\alpha$  between pump and signal, one can choose to set the two beams at a suitable angle, according to the desired bandwidth. For  $\alpha \approx 2.5^\circ$ , for instance, the bandwidth acceptance of the amplifier allows to get pulses about 15 fs long after compression [49]; in this case tunability can be achieved by tilting the

crystal towards the desired  $\theta_m$ . Fig. 14(b) shows a series of spectra acquired in this configuration for different values of  $\theta_m$ , demonstrating the continuous tunability of the setup. The bandwidth can be changed without any consequence on the pulse chirp, thus avoiding any changes in the compressor configuration.

#### 8. *OPAs with carrier-envelope-phase stabilization*

Ultrabroadband light pulses containing only a few optical carrier cycles under their envelope are currently produced by several methods, including direct generation from a mode-locked oscillator [50], spectral broadening in a guiding medium [51] and optical parametric amplification (see previous Section). For such short pulses, the maximum amplitude of the electric field varies significantly between consecutive optical half-cycles, so that it becomes important to control the evolution of the electric field underneath the pulse envelope. Mathematically, the electric field of an ultrashort pulse can be written as

$$E(t) = A(t) \cos(\omega_c t + \phi) \quad (46)$$

where  $A(t)$  is the pulse envelope with its maximum at  $t = 0$ ,  $\omega_c$  is the carrier frequency and  $\phi$  is the so-called carrier-envelope phase (CEP). If  $\phi = 0$ , a maximum of the electric field corresponds to the peak of the pulse envelope (cosine pulse), while if  $\phi = \pi/2$  the electric at the peak of the pulse envelope is zero (sine pulse). Control of the CEP becomes important for extreme nonlinear optics experiments which are sensitive to the electric field rather than the intensity of the pulse. Examples of such effects in the non-resonant case, requiring high pulse energies, are above-threshold ionization [52] and high-harmonic generation [53], for which CEP-control is a prerequisite to the production of attosecond pulses [54].

A mode-locked laser oscillator produces a pulse train in which the CEP changes from pulse to pulse, due to the difference between phase velocity (with which the carrier propagates) and group velocity (with which the envelope propagates) during one roundtrip. The pulse-to-pulse CEP

slippage  $\Delta\phi$ , in addition, is not constant in time, but drifts due to fluctuations in the cavity parameters. CEP stabilization methods can be divided into active and passive ones.

Active methods rely on the fact that a femtosecond mode-locked oscillator emits a frequency comb [55], i.e. a superposition of longitudinal modes with frequencies:  $\nu_n = \nu_{CEO} + n\nu_R$ , where  $\nu_R$  is the laser repetition rate and  $\nu_{CEO}$  is the so-called carrier-envelope offset frequency, related to  $\Delta\phi$  by:

$$\nu_{CEO} = \frac{\Delta\phi}{2\pi}\nu_R. \quad (47)$$

Generation of actively CEP-stabilized pulses can then be accomplished in three steps: (i) measurement of  $\nu_{CEO}$  by a nonlinear interferometer; (ii) stabilization of  $\nu_{CEO}$  by active feedback on the oscillator; (iii) picking of pulses at a fraction of  $\nu_{CEO}$ , so that their CEP becomes reproducible from shot to shot. The selected CEP-stable pulses are then amplified either in a solid-state amplifier or in an OPA, and a second electronic feedback loop is required to compensate for CEP fluctuations induced by the amplification process.

Passive methods, pioneered by Baltuska *et al.* [56], are based on the process of DFG, in which two pulses at frequencies  $\omega_2$  and  $\omega_3$  are mixed in a second-order nonlinear crystal to generate the difference frequency (DF):  $\omega_1 = \omega_3 - \omega_2$ . The CEPs of the three pulses are linked through the parametric interaction by the relationship:  $\phi_1 = \phi_3 - \phi_2 - \pi/2$ . If the two pulses undergoing the DFG process are derived from the same source and thus share the same CEP ( $\phi_3 = \phi + c_3$ ,  $\phi_2 = \phi + c_2$ ), then  $\phi_1 = c_3 - c_2 - \pi/2 = \text{const.}$ , i.e. the fluctuations of  $\phi$  are automatically cancelled in a passive, all-optical way.

Based on these considerations, it is easy to understand that in a white-light seeded OPA, in which the pump and the seed are derived from the same source, the idler is automatically phase-stabilized [56-58]. The physical mechanisms underlying this effect are basically three: (i) a white light continuum generated by SPM maintains the same value of CEP as the driving pulse; (ii) the OPA process preserves the CEP of the seed pulse, carrying it to the signal wave; (iii) in an OPA, the

idler is produced by DFG between pump and signal, so that the CEPs of the two pulses add up with different signs. Let us now consider the case in which both pump and seed are derived from the same pulse: in this situation their CEPs are equal and thus cancel in the idler beam, leading to phase stabilization.

If we consider previously described OPA configurations, those pumped by the FW satisfy this condition, because the 800-nm beam is used both for seed generation and as a pump [58]; on the other hand, the visible NOPA does not satisfy this condition, because the pump is the SH and carries CEP  $2\varphi$  while the seed is generated by the FW and carries CEP  $\varphi$ . To solve this problem, Baltuska *et al.* built a NOPA in which the white light seed is generated by the SH instead of the FW, in a CaF<sub>2</sub> plate [56, 57]; in this case, both pump and signal carry a CEP  $2\varphi$  and the idler is self phase stabilized. Since the idler of the NOPA spans over an octave of bandwidth, its self-frequency-stabilization can be simply verified by a nonlinear  $f$ -to- $2f$  interferometer [59]. The pioneering work by Baltuska *et al.* suffers from the disadvantage that the self-phase-stabilized idler pulses obtained from the NOPA idler have a strong angular dispersion, because of the non-collinear phase matching geometry. To solve this problem, passive CEP stabilization by DFG between pulses generated by two OPAs sharing the same CEP was also demonstrated [60], obtaining self-phase-stabilized pulses free from angular dispersion and with ultrabroad bandwidth spanning over an octave, from 800 to 1700 nm. However in this configuration the generated pulse energies are quite low, being limited to 200 nJ. These are all inter-pulse DFG schemes, as they involve mixing of two separate frequency-shifted pulses, synchronized by a delay line; in this case, any fluctuation of the path-length difference will induce a CEP jitter. A more robust approach is based on an intra-pulse scheme, in which DFG is achieved between long and short wavelength components of a single ultrabroadband pulse [61]; in this configuration the two pulses undergoing the DFG process are automatically synchronized and delay-induced CEP jitter is suppressed. This CEP-stabilized DFG seed can then be amplified by one or more OPA stages [62, 63].

Here we describe a setup [64] (see Fig. 15) which is driven by a CPA Ti:sapphire system (1.5 mJ, 50 fs, 1 kHz): the seed, generated by DFG of a hollow-fiber-broadened supercontinuum, is amplified by an OPA pumped by the FF of Ti:sapphire and operated around degeneracy. A fraction of the energy ( $\sim 250 \mu\text{J}$ ) is coupled in a 60-cm long, 300- $\mu\text{m}$  inner diameter hollow fiber filled with krypton (0.7 bar pressure) to generate a broadband supercontinuum by self-phase-modulation. The outcoupled pulses, with 200- $\mu\text{J}$  energy and spectrum extending from 650 to 1000 nm, are compressed by ultrabroadband chirped mirrors, in order to acquire a slightly negative chirp and optimise the subsequent DFG process. The pulses are then focused by a 1500 mm radius spherical mirror onto a 200  $\mu\text{m}$  thick  $\beta$ -barium borate (BBO) crystal cut for DFG with type II [ $e+o(\text{DFG}) \rightarrow e$ ] phase matching ( $\theta = 32^\circ$ ,  $\varphi = 30^\circ$ ). DFG takes place between different frequency components of the supercontinuum; for a given crystal orientation, different pairs of frequencies can be phase-matched simultaneously, giving rise to a broad DF spectrum even for a relatively thick crystal. For an intensity of  $100 \text{ GW}/\text{cm}^2$ , just below the onset of third-order nonlinear processes in the crystal, vertically polarized DF pulses with energy up to 20 nJ are produced. The bandwidth and central wavelength of the DF pulses can be controlled by acting on the crystal phase-matching angle and the pulse chirp, fine tuned by a pair of thin glass wedges; a typical spectrum, shown in Fig. 16 as a solid line, corresponds to a TL pulse duration of 6 fs. A thin gelatine polarizer is used to suppress the residual supercontinuum collinear with the DF pulses, without introducing any significant amount of dispersion; also, to prevent chirping of the DF pulses, they are handled exclusively by reflective optics.

The DF pulses are used to seed a two-stage OPA pumped by the residual, 750- $\mu\text{J}$  800 nm light. The first stage is pumped by 250  $\mu\text{J}$  and uses a 2 mm thick BBO crystal cut for type I phase matching ( $\theta = 21^\circ$ ); it produces pulse energies up to 3.5  $\mu\text{J}$  with a spectrum (dashed line in Fig. 16) almost as broad as that of the DF pulses. A type I OPA operated around degeneracy displays in fact a broad phase-matching bandwidth, due to the group-velocity matching between signal and idler (see

Section 4). Both OPA stages we use a non-collinear geometry with a small angle ( $\approx 1.5^\circ$ ) between pump and seed to facilitate combination and separation of the beams and to prevent signal-idler interference. The second OPA stage is pumped by 1 mJ and uses a 3 mm thick BBO cut for type II phase matching ( $\theta = 28.5^\circ$ ,  $\varphi = 30^\circ$ ); this configuration is chosen because, due to its narrower gain bandwidth, it allows to control the amplified pulse spectrum and generate pulses with TL duration. When driven into saturation, the second OPA stage generates pulses with 200- $\mu$ J energy. Both OPA stages are operated in a regime in which parametric superfluorescence, once the DF seed is blocked, is negligible; this is important because any superfluorescence background would not be phase-stabilized and would thus degrade the CEP stability of the system.

The amplified pulses are expected to be close to a TL duration without the need of any compression. In fact the DF pulses are generated by a  $\approx 10$  fs pulse and are expected to have a comparable time duration. The contribution to dispersion due to the propagation in the BBO crystals used for the NOPA stages can be minimized by tuning the central wavelength of the amplified pulses around 1.55  $\mu$ m, where BBO exhibits zero second-order dispersion. The pulse width after the second stage, measured by a collinear autocorrelator, is 15-fs, which is very close to the TL value and corresponds to  $\approx 3$  cycles of the carrier wavelength.

The CEP stability of the amplified pulses was verified and characterized by an  $f$ -to- $2f$  interferometer. A suitably attenuated fraction of the pulse energy is first focused in a 2 mm thick sapphire plate, to generate a white light continuum, and then frequency doubled in a 100  $\mu$ m thick BBO crystal. The spatially overlapped FW and SH are sent to a spectrometer through a polarizer. In the 700-800 nm wavelength range, the spectrally broadened FW and the SH are overlapped; by adjusting their relative intensities with the polarizer, an interference pattern is observed, according to the expression:

$$I(\omega) = I_{FW}(\omega) + I_{SH}(\omega) + 2\sqrt{I_{FW}(\omega)I_{SH}(\omega)} \cos(\omega\tau + \phi) \quad (48)$$

where  $\tau$  is the delay between FW and SH pulses and  $\phi$  is the CEP to be characterized. If the CEP is not stable, the fringes will move from shot to shot and will vanish upon averaging. Fig. 17 shows, as a solid line, an interferogram acquired by averaging over 200 shots; the appearance of an high-contrast fringe pattern is a clear demonstration of CEP stabilization. To prove that the fringes stem from FW-SH interference and do not have any spurious origin, we inserted an 6 mm thick BK7 plate before the SH crystal. The plate is expected to increase, due to dispersion, the delay between the 800 and 1600 nm components, and thus decrease the fringe period, as observed in Fig. 17, dashed line. By taking Fourier transforms of the oscillatory components of the interferograms (see inset of Fig. 17) one finds an increase in delay by 206 fs, in excellent agreement with the calculated 204 fs group delay introduced by the plate.

#### 9. *Optical parametric chirped pulse amplification (OPCPA)*

There is a great interest in the generation of ever increasing laser peak powers and focused intensities, for a number of current and potential applications. Using the CPA technique, peak powers in excess of 1 PW [65] and intensities greater than  $10^{21}$  W/cm<sup>2</sup> have been demonstrated; to scale this performance to even higher levels, a number of issues must be faced in conventional CPA systems. Since the energy levels are approaching the damage threshold of the compressor gratings, significant increases of the peak power can be only achieved by shortening the pulse duration, which in turn requires an increase of the gain bandwidth. For strongly driven amplifying media, however, the phenomenon of gain narrowing reduces the available bandwidth. In addition, the prepulse due to amplified spontaneous emission (ASE) spoils the temporal pulse contrast, and the large linear and nonlinear phases accumulated in the long paths through the amplifying media prevent transform-limited pulse recompression and diffraction-limited focusing. A novel high power amplification scheme, solving most of these problems, was recently proposed [66], and termed “optical parametric chirped pulse amplification” (OPCPA). In this scheme parametric gain is achieved by coupling a quasi-monochromatic high energy pump field (such as, for example, a

picosecond or nanosecond pulse generated by a neodymium laser) to a chirped, low energy broadband seed field in a nonlinear crystal [67-69]. If the seed pulse is sufficiently stretched, good energy extraction from the pump field can be achieved, and subsequent recompression makes it possible to reach very high peak powers. The OPCPA concept has some very important advantages with respect to the standard CPA:

1) the parametric amplification process, in the non-collinear geometry, can provide gain bandwidths well in excess of those achievable with conventional amplifiers and could sustain pulse spectra corresponding to a transform-limited duration of  $\approx 5$  fs. High energies are possible by using large nonlinear crystals, such as potassium dihydrogen phosphate (KDP), which can be grown to sizes of tens of centimeters. These crystals should be capable of withstanding pump energies of hundreds of joules.

2) the OPCPA has the capability of providing a high gain in a relatively short path; for example, a lithium triborate (LBO) crystal pumped by 0.5 ns pulses at  $0.526 \mu\text{m}$ , at intensities below the damage threshold, can have a gain coefficient of  $12 \text{ cm}^{-1}$ . This short path length allows a compact, tabletop amplifier setup and also minimizes the linear and nonlinear phase distortions and ensures an excellent temporal and spatial quality of the pulses.

3) in OPCPA amplification occurs only during the pump pulse, so that the ASE and the consequent prepulse pedestal are greatly reduced.

4) in a standard amplifier, even for good energy extraction, there is always some thermal loading, due to the quantum defect (difference between energies of the pump and emitted photons, usually absorbed by the material in non-radiative decay processes); this becomes very relevant for high energy amplifiers, often requiring cryogenic cooling. In OPCPA, on the other hand, no fraction of the pump photon energy is deposited in the medium, because it is transformed in the sum of the signal and idler photon energies; so thermal loading effects, apart from parasitic absorption, are completely absent, greatly reducing spatial aberration effects on the beams.

The OPCPA concept is very promising and has been already implemented in a proof-of-principle experiment to generate TW-level pulses [69]; in a low repetition rate systems pumped by a Nd:glass laser chain, pulses with energy up to 570 mJ with 115 fs duration, corresponding to a peak power of 3.67 TW, have been obtained [70]. More recently, the ultrabroad gain bandwidth obtainable from OPCPA has been exploited to generate 8-mJ pulses with 100-THz bandwidth [71], subsequently recompressed to 5-mJ, 10-fs pulses. The system was pumped by a frequency-doubled, amplified Nd:YAG laser producing 60-mJ, 60-ps pulses at 20 Hz repetition rate and 532 nm wavelength, and seeded by a broadband Ti:sapphire oscillator; parametric gain was achieved in two 4-mm type I BBO crystals. In addition, since OPAs preserve the CEP of the seed beam, it is possible to achieve phase-stable amplification of ultrashort pulses; recently, 11.8-fs, 120- $\mu$ J pulses at 1 kHz have been obtained [72, 73].

Future developments include the use of OPCPA pumped by large-frame high energy lasers, in order to generate PW-class pulses. As an example, the design for an OPCPA pumped by the high-power iodine laser Asterix IV is given in Ref. [74]. The Asterix IV pump laser delivers at the fundamental wavelength (1.315  $\mu$ m) up to 1.2 kJ of energy in pulses with a duration of 500 ps; the beam can be efficiently frequency tripled to produce over 500 J of energy at 0.438  $\mu$ m. The 10-fs seed pulses are generated by a Ti:sapphire oscillator and then stretched to several hundreds picoseconds; parametric amplification takes place in three stages, using a non-collinear interaction geometry, and telescopes increase the beam size after each stage. The first two stages employ LBO because of its high nonlinear coefficient and broad amplification bandwidth, while the last stage uses KDP because this nonlinear crystal can be grown in the large sizes ( $\approx$  30 cm) required to keep the fluence below the damage threshold. After the compressor, energies of 100 J with pulse duration of 20 fs are expected, corresponding to a peak power of 5 PW and to a focused intensity of  $10^{23}$  W/cm<sup>2</sup>.

## 10. Conclusions

Ultrafast OPAs are a mature technology, making it possible to extend considerably the tuning range of femtosecond Ti:sapphire laser systems. Several OPA designs have become standard and are commercially available. In particular, near-IR OPAs (pumped by the FW of a Ti:sapphire laser) offer tunability from 1.1 to 2.5  $\mu\text{m}$  with several tens of  $\mu\text{J}$  energy, while visible OPAs (pumped by the SH of a Ti:sapphire laser) are tunable from 0.45 to 2.5  $\mu\text{m}$  with somewhat lower energies. Typical pulsewidths obtainable from these systems are in the 50-200 fs range, depending on the specific design and the pump pulse duration. SFG and DFG techniques allow extending their tunability from the UV range to the mid-IR, out to 12  $\mu\text{m}$ .

In addition to their standard application as continuously frequency tunable optical amplifiers, OPAs have some other remarkable properties that make them useful in ultrafast optics:

- a) under some conditions, in particular in a non-collinear interaction geometry, OPAs offer very broad gain bandwidths, thus enabling the generation of very short pulses, down to a few optical cycles. Such pulse durations are much shorter than that of the driving pulse, so that OPAs act as effective pulse compressors.
- b) The DFG process which takes place in the OPA leads to a subtraction of the carrier-envelope phases of pump and signal pulses. Therefore, if pump and signal carry the same CEP, the idler pulses are automatically self-phase-stabilized. This passive, all-optical self-phase-stabilization technique, in conjunction with the broad phase matching bandwidths of OPAs, offers an interesting route to the generation of few-optical-cycles with precisely controlled electric fields.
- c) OPAs also have the capability of providing very high gains over broad bandwidths: these characteristics, together with the relatively short material path, negligible thermal loading of the crystals, low linear and nonlinear phase distortions and low levels of amplified spontaneous emission, make them very attractive candidates for large-scale, high peak power amplifiers. The

OPCPA concept holds promise to increase the peak powers available from lasers well above the current limit of 1 PW.

## Figure Captions

**Figure 1 :** schemes of the SFG and DFG processes and their interpretation in terms of excitation of virtual levels.

**Figure 2:** (a) parametric gain for an OPA at the pump wavelength  $\lambda_p = 0.8 \mu\text{m}$  and the signal wavelength  $\lambda_s = 1.2 \mu\text{m}$ , using type I phase matching in BBO ( $d_{\text{eff}} = 2 \text{ pm/V}$ ). (b) parametric gain for an OPA at the pump wavelength  $\lambda_p = 0.4 \mu\text{m}$  and the signal wavelength  $\lambda_s = 0.6 \mu\text{m}$ , using type I phase matching in BBO ( $d_{\text{eff}} = 2 \text{ pm/V}$ ).

**Figure 3:** phase matching angle as a function of wavelength for a BBO OPA pumped at  $0.8 \mu\text{m}$  for type I phase matching (dashed line), type II phase matching (signal extraordinary, dash-dotted line) and type II phase matching (idler extraordinary, solid line).

**Figure 4:** pump-signal ( $\delta_{\text{sp}}$ ) and pump-idler ( $\delta_{\text{ip}}$ ) group velocity mismatch curves for a BBO OPA pumped at  $0.8 \mu\text{m}$  for type I phase matching (solid lines) and type II phase matching (idler extraordinary, dashed lines).

**Figure 5:** pump-signal ( $\delta_{\text{sp}}$ ) and pump-idler ( $\delta_{\text{ip}}$ ) group velocity mismatch curves for a BBO OPA pumped at  $0.4 \mu\text{m}$  for type I phase matching (solid lines) and type II phase matching (idler extraordinary, dashed lines).

**Figure 6:** Phase matching bandwidth for a BBO OPA pumped at  $0.8 \mu\text{m}$  for type I phase matching (solid line) and type II phase matching (idler extraordinary, dashed line). Crystal length is  $4 \text{ mm}$  and pump intensity  $50 \text{ GW/cm}^2$ .

**Figure 7:** Phase matching bandwidth for a BBO OPA pumped at 0.4  $\mu\text{m}$  for type I phase matching (solid line) and type II phase matching (idler extraordinary, dashed line). Crystal length is 2 mm and pump intensity 100  $\text{GW}/\text{cm}^2$ .

**Figure 8:** scheme of an ultrafast optical parametric amplifier. BS, beam splitter; OPA, optical parametric amplification stage.

**Figure 9:** scheme of a near-IR OPA. BS, beam splitter; DF, dichroic filter; DM, dichroic mirror.

**Figure 10:** scheme of a mid-IR pulse generation stage. DM, dichroic mirrors; LPF, long-pass filter.

**Figure 11:** (a) schematic of a non-collinear interaction geometry; (b) representation of signal and idler pulses in the case of collinear interaction; and (c) same as (b), for non-collinear interaction.

**Figure 12:** phase matching angle as a function of signal wavelength for a non-collinear type I BBO OPA pumped at 0.4  $\mu\text{m}$ , as a function of pump-signal angle  $\alpha$ .

**Figure 13:** scheme of a non-collinear OPA pumped at 0.4  $\mu\text{m}$ . BPF, bandpass filter.

**Figure 14:** (a) NOPA spectrum under optimum alignment conditions (pump-signal angle  $\alpha = 3.7^\circ$ ); (b) spectra generated by the NOPA with  $\alpha = 2^\circ$ , demonstrating continuous tunability.

**Figure 15:** Experimental setup for the generation of high-energy self-phase-stabilized pulses; Ti:Sa, CPA Ti:sapphire laser; DFG, 200  $\mu\text{m}$  thick BBO crystal; POL, thin film polarizer.

**Figure 16:** Normalized spectra of the DF pulses (solid line) and of the pulses after the first (dashed line) and second (dotted line) OPA stages.

**Figure 17:** Spectral interference patterns between FW and SH as generated (a) and with a 5.9 mm thick BK7 plate on the beam path (b). The inset shows the Fourier transforms of the oscillatory components of the interferograms.

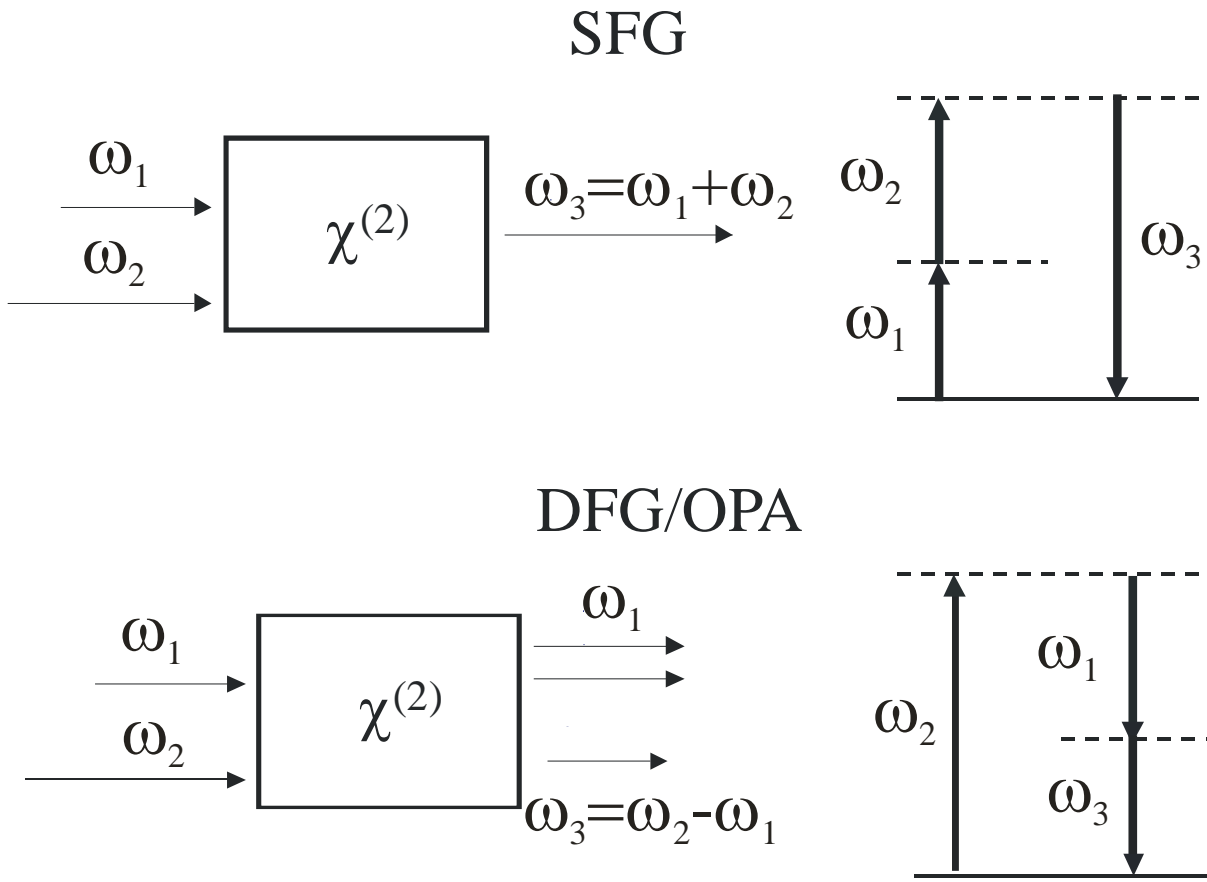


Figure 1

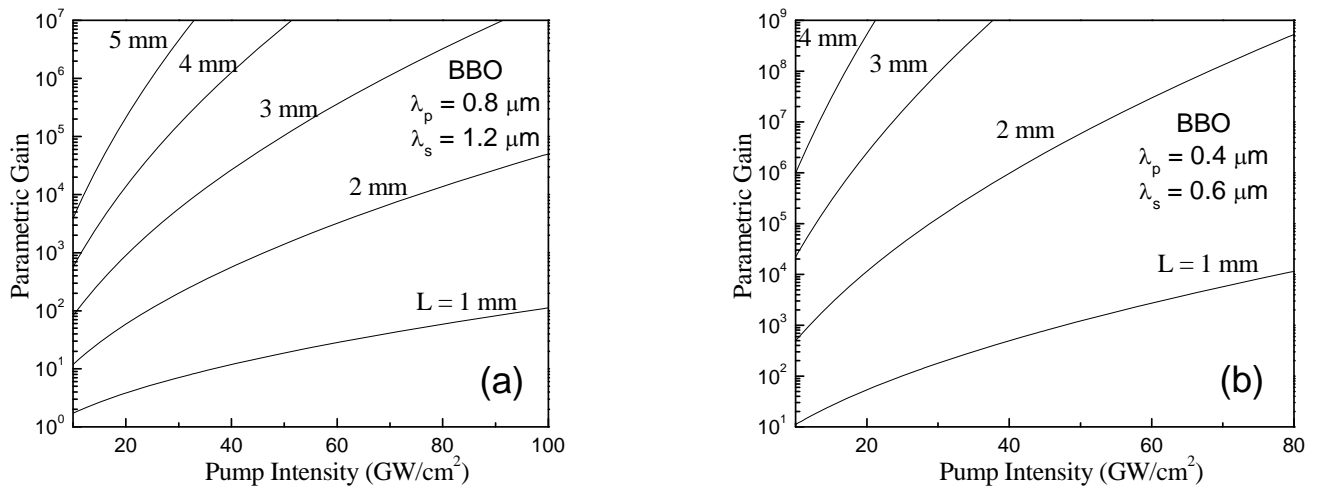


Figure 2

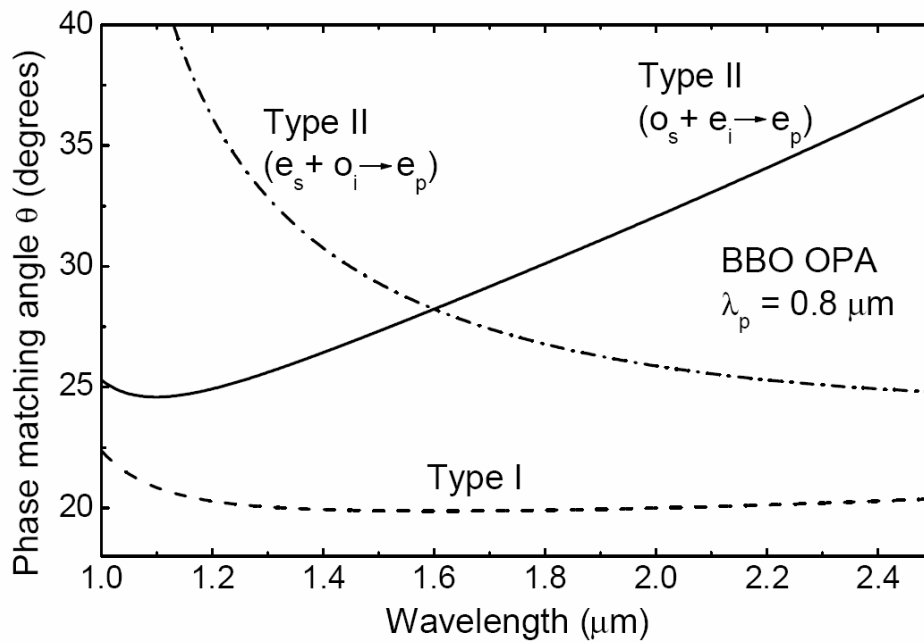


Figure 3

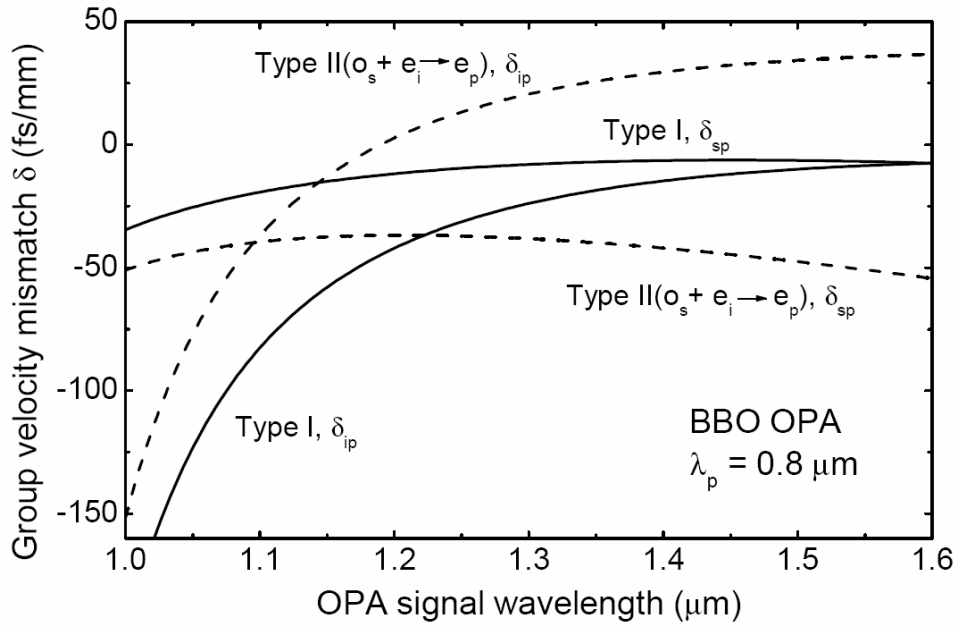


Figure 4

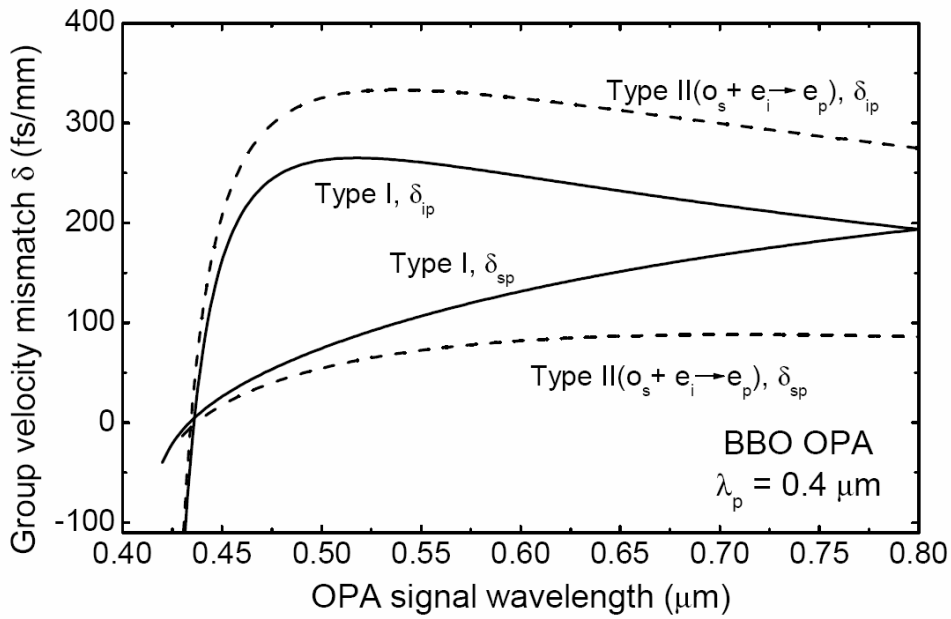


Figure 5

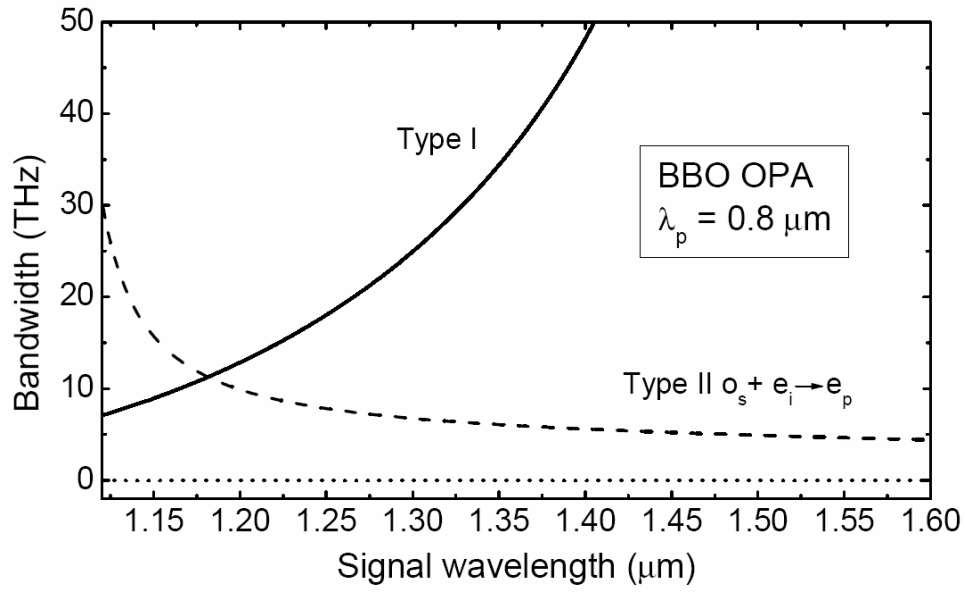


Figure 6

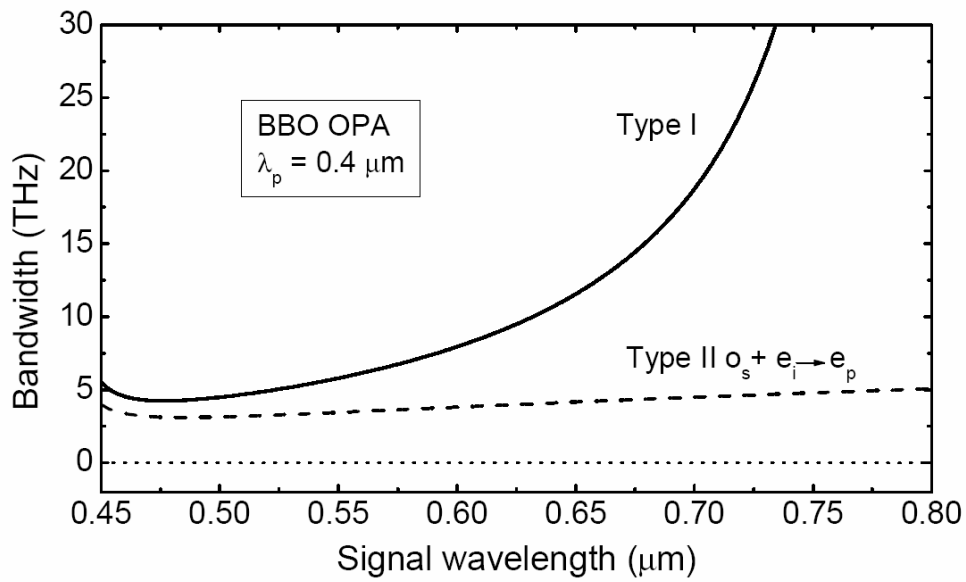


Figure 7

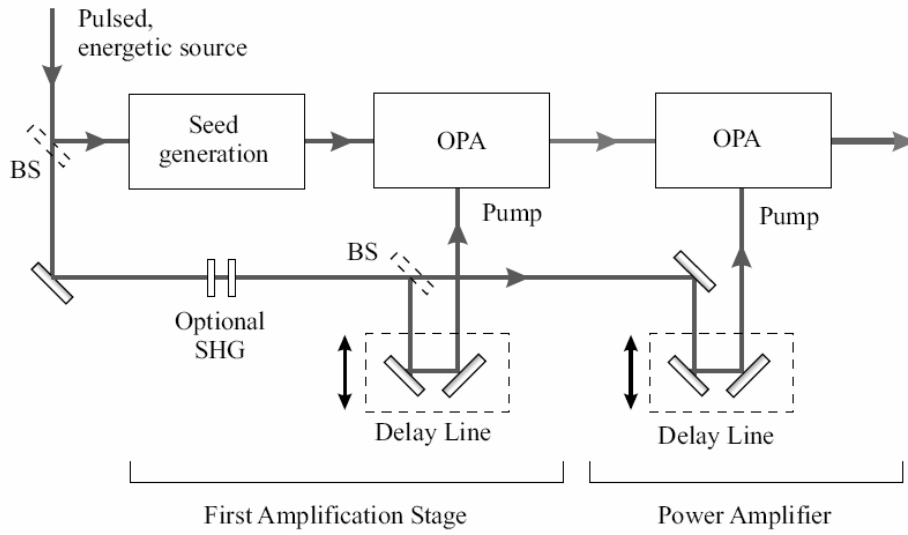


Figure 8

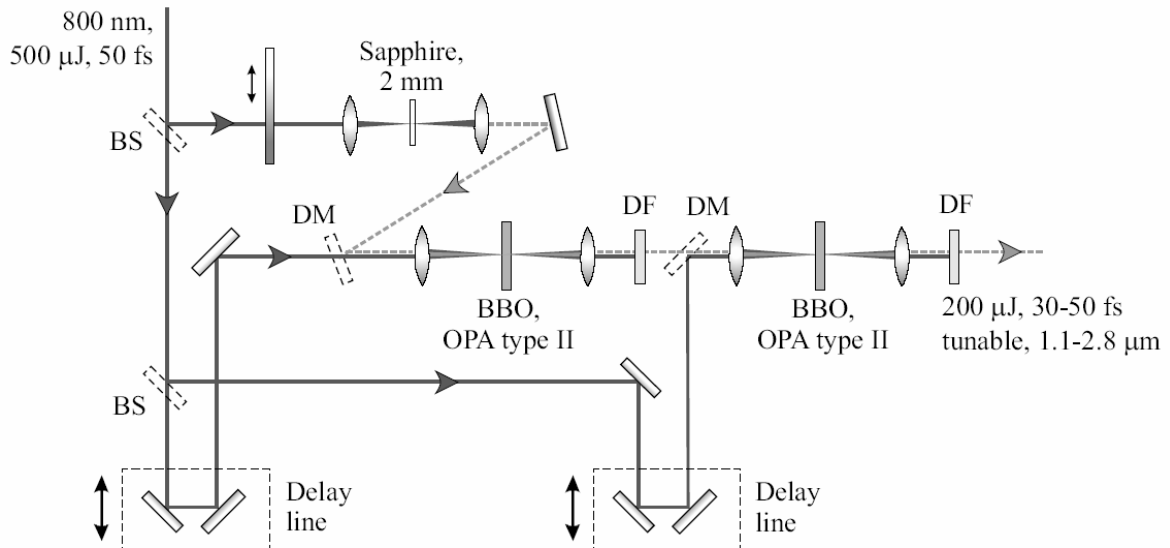


Figure 9

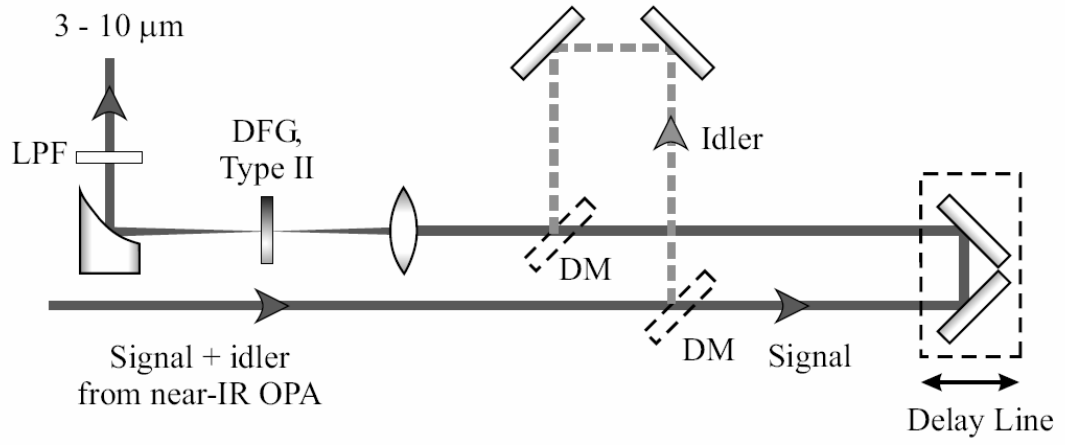


Figure 10

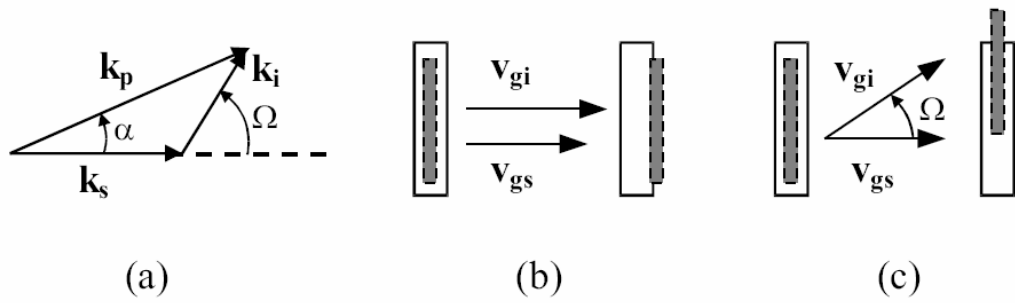


Figure 11

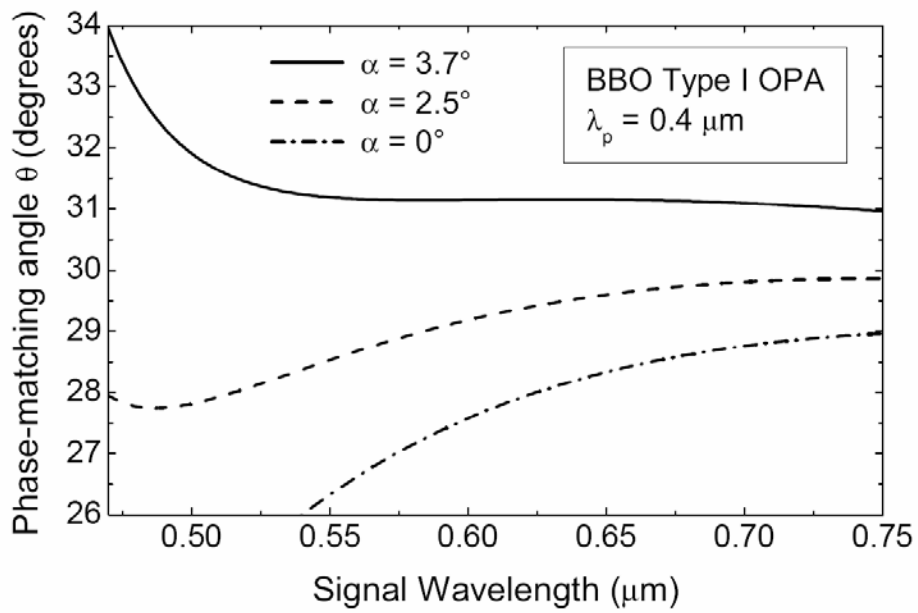


Figure 12

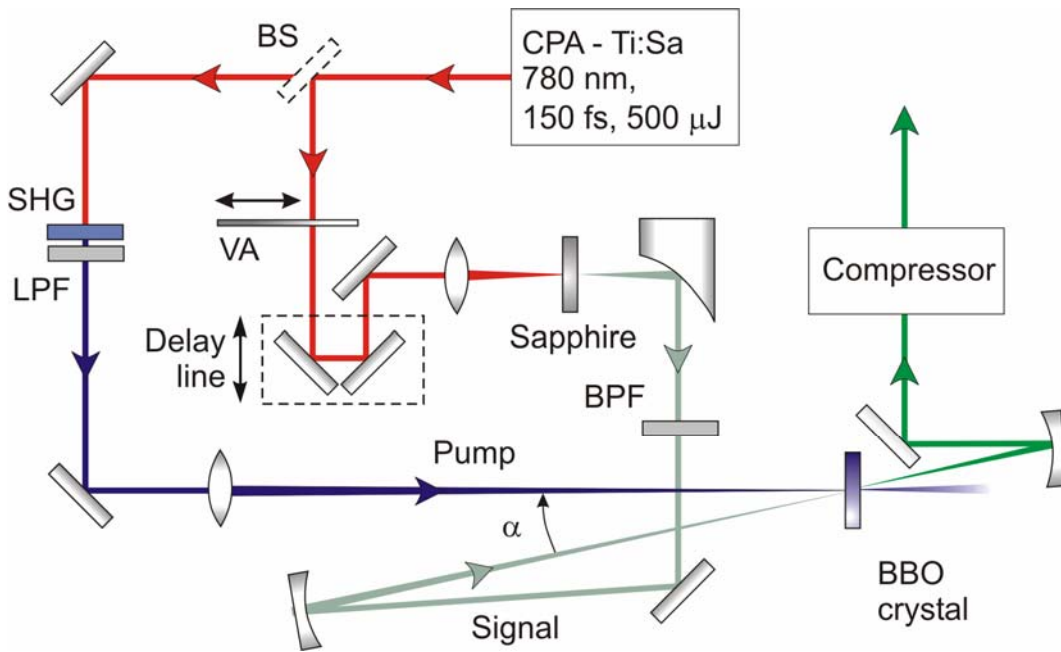


Figure 13

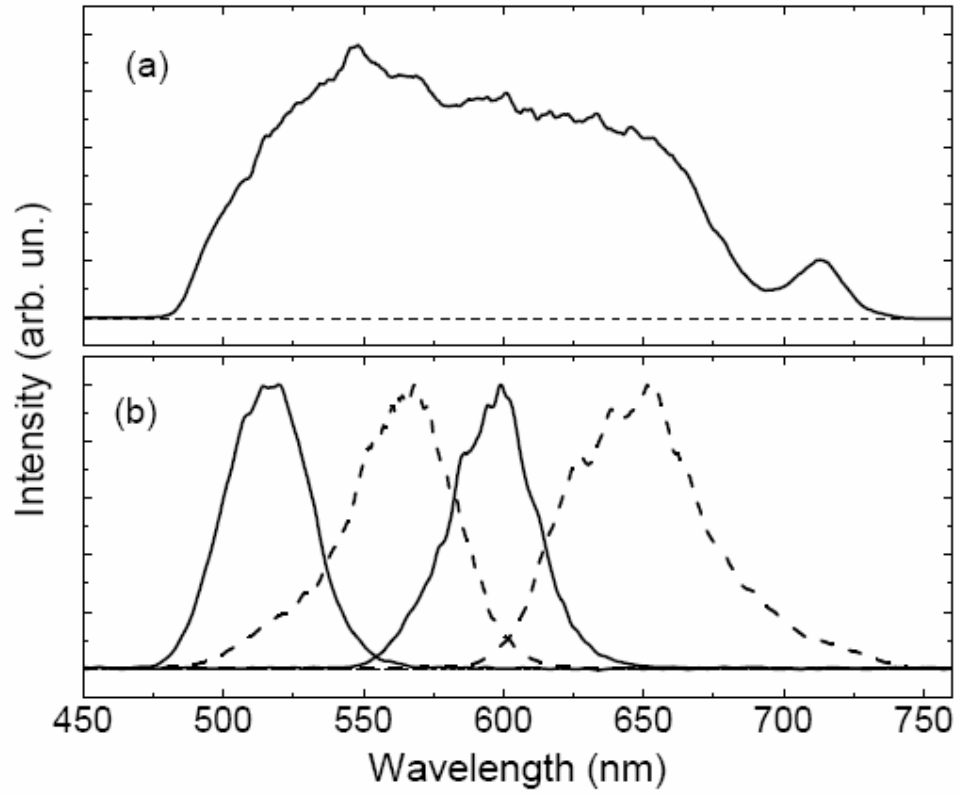


Figure 14

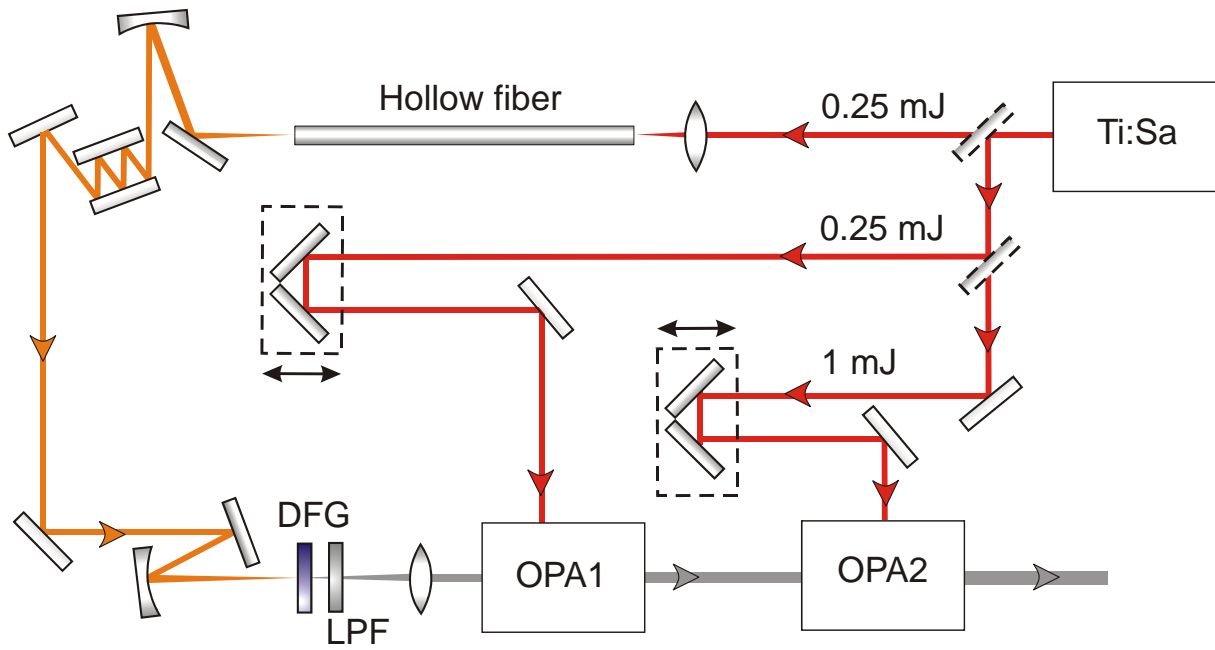


Figure 15

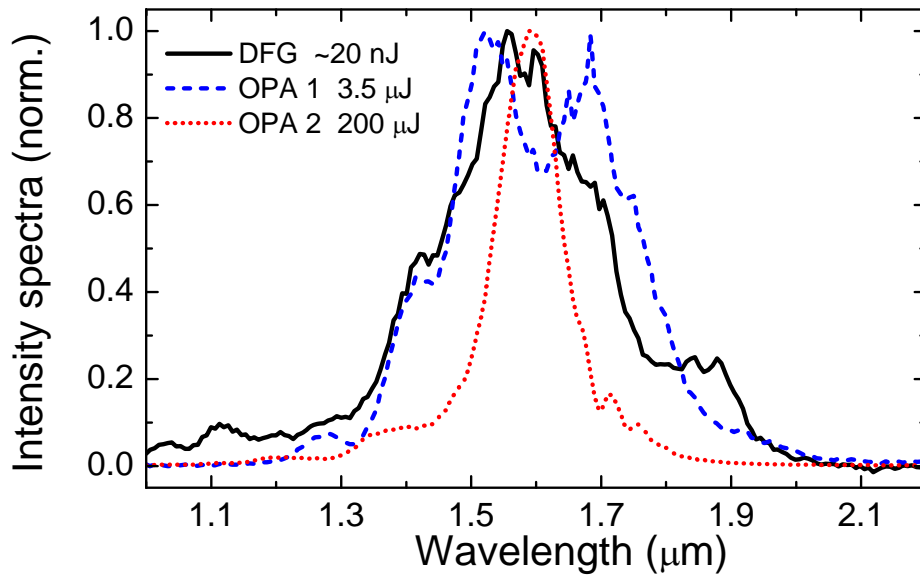


Figure 16

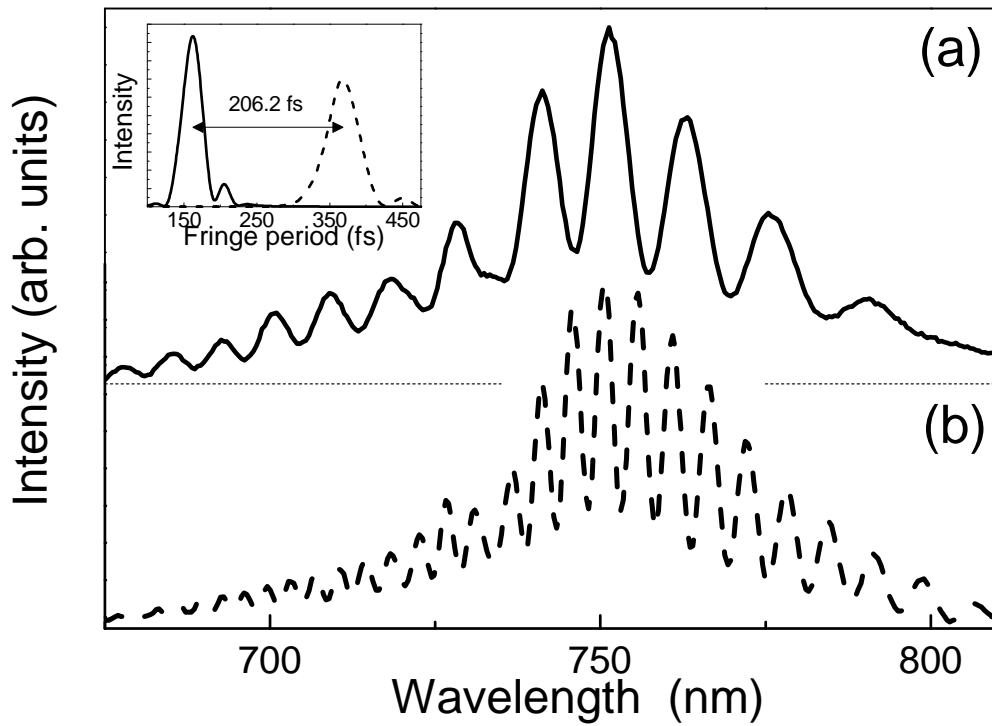


Figure 17

## References

1. A.H. Zewail, J. Phys. Chem. A **104**, 5660 (2000).
2. D.E. Spence, P.N. Kean, and W. Sibbett, Opt. Lett. **16**, 42 (1991).
3. S. Backus, C. G. Durfee III, M. M. Murnane, and H. C. Kapteyn, Rev. Sci. Instrum. **69**, 1207 (1998).
4. J.A. Giordamaine and R.C. Miller, Phys. Rev. Lett. **14**, 973 (1965).
5. R.L. Byer and R.L. Herbst, in *Nonlinear Infrared Generation*, Y. R. Shen, ed. (Springer-Verlag, Berlin, 1977), p. 96.
6. R.A. Baumgartner and R.L. Byer, IEEE J. Quantum Electron. **15**, 432 (1979).
7. Y.R. Shen, *The Principles of Nonlinear Optics* (John Wiley & Sons, New York, 1984).
8. R. Boyd, *Nonlinear Optics* (Academic, New York, 1992).
9. E. S. Wachman, D. C. Edelstein, and C. L. Tang, Opt. Lett. **15**, 136 (1990).
10. Q. Fu, G. Mak, and H.M. van Driel, Opt. Lett. **17**, 1006 (1992).
11. W.S. Pelouch, P.E. Powers, and C.L. Tang, Opt. Lett. **17**, 1070 (1992).
12. P. E. Powers, R. J. Ellingson, W. S. Pelouch, and C. L. Tang, JOSA B **10**, 2162 (1993).
13. G. Cerullo and S. De Silvestri, Rev. Sci. Instrum. **74**, 1 (2003).
14. V.G. Dmitriev, G.G. Gurzadyan, and D.N. Nikogosyan, *Handbook of Nonlinear Optical Crystals*, Springer Verlag, Berlin, 1991.
15. S. E. Harris, M. K. Oshman, and R. L. Byer, Phys. Rev. Lett. **18**, 732 (1967).
16. R.R. Alfano, ed., *The Supercontinuum Laser Source*, Springer-Verlag, New York, 1989.
17. J.K. Ranka and A.L. Gaeta, Opt. Lett. **23**, 534 (1998).
18. A.L. Gaeta, Phys. Rev. Lett. **84**, 3582 (2000).
19. W. Joosen, P. Agostini, G. Petite, J.P. Chambaret, A. Antonetti, Opt. Lett. **17**, 133 (1992).
20. G.P. Banfi, P. Di Trapani, R. Danielius, A. Piskarkas, R. Righini, I. Sa'nta, Opt. Lett. **18**, 1547 (1993).

- 
21. G.P. Banfi, R. Danielius, A. Piskarkas, P. Di Trapani, P. Foggi, R. Righini, *Opt Lett.* **18**, 1633 (1993).
  22. F. Seifert, V. Petrov, F. Noack, *Opt Lett.* **19**, 837 (1994).
  23. V. Petrov, F. Seifert, F. Noack, *Appl. Phys. Lett.* **65**, 268 (1994).
  24. M. Nisoli, S. De Silvestri, V. Magni, O. Svelto, R. Danielius, A. Piskarkas, G. Valiulis, and A. Varavinicius, *Opt. Lett.* **19**, 1973 (1994).
  25. M. Nisoli, Stagira, S. De Silvestri, O. Svelto, G. Valiulis, and A. Varavinicius, *Opt. Lett.* **23**, 630 (1994).
  26. V.V. Yakovlev, B. Kohler, and K.R. Wilson, *Opt. Lett.* **19**, 2000 (1994).
  27. K.R. Wilson and V.V. Yakovlev, *J. Opt. Soc. Am. B* **14**, 444 (1997).
  28. M.K. Reed, M.K. Steiner-Shepard, and D.K. Negus, *Opt. Lett.* **19**, 1855 (1994).
  29. M. K. Reed, M.S. Armas, M. K. Steiner-Shepard, and D. K. Negus, *Opt. Lett.* **20**, 605 (1995).
  30. S.R. Greenfield and M.R. Wasielewski, *Opt. Lett.* **20**, 1394 (1995).
  31. P. Di Trapani, A. Andreoni, C. Solcia, G.P. Banfi, R. Danielius, A. Piskarskas, and P. Foggi, *J. Opt. Soc. Am. B* **14**, 1245 (1997).
  32. T.S. Sosnowski, P.B. Stephens, and T.B. Norris, *Opt. Lett.* **21**, 140 (1996).
  33. K.S. Wong, Z.R. Qui, H. Wang, and G.K.L. Wong, *Opt. Lett.* **22**, 898 (1997).
  34. F. Seifert, V. Petrov, and M. Woerner, *Opt. Lett.* **19**, 2009 (1994).
  35. M. K. Reed and M. K. Steiner Shepard, *IEEE J. Quantum Electron.* **32**, 1273 (1996).
  36. B. Golubovic and M.K. Reed, *Opt. Lett.* **23**, 1760 (1998).
  37. G.M. Gale, M. Cavallari, T.J. Driscoll, and F. Hache, *Opt. Lett.* **20**, 1562 (1995).
  38. G.M. Gale, M. Cavallari, and F. Hache, *JOSA B* **15**, 702 (1998).
  39. T. Wilhelm, J. Piel, and E. Riedle, *Opt. Lett.* **22**, 1494 (1997)
  40. G. Cerullo, M. Nisoli, and S. De Silvestri, *Appl. Phys. Lett.* **71**, 3616 (1997).
  41. A. Shirakawa and T. Kobayashi, *Appl. Phys. Lett.* **72**, 147 (1998).

- 
42. G. Cerullo, M. Nisoli, S. Stagira, and S. De Silvestri, *Opt. Lett.* **23**, 1283 (1998).
  43. A. Shirakawa, I. Sakane, and T. Kobayashi, *Opt. Lett.* **23**, 1292 (1998).
  44. M. Zavelani-Rossi, G. Cerullo, S. De Silvestri, L. Gallmann, N. Matuschek, G. Steinmeyer, U. Keller, G. Angelow, V. Scheuer, and T. Tschudi, *Opt. Lett.* **26**, 1155 (2001).
  45. A. Baltuska, T. Fuji, and T. Kobayashi, *Opt. Lett.* **27**, 306 (2002).
  46. A. Shirakawa, I. Sakane, M. Takasaka, and T. Kobayashi, *Appl. Phys. Lett.* **74**, 2668 (1999).
  47. P. Baum, M. Breuer, E. Riedle, and G. Steinmeyer, *Opt. Lett.* **31**, 2220 (2006)
  48. M. R. Armstrong, P. Plachta, E. A. Ponomarev, and R. J. D. Miller, *Opt. Lett.* **26**, 1152 (2001).
  49. C. Manzoni, D. Polli, and G. Cerullo, *Rev. Sci. Instrum.* **77**, 023103 (2006).
  50. R. Ell, U. Morgner, F. X. Kaertner, J. G. Fujimoto, E. P. Ippen, V. Scheuer, G. Angelow, T. Tschudi, M. J. Lederer, A. Boiko, and B. Luther-Davies, *Opt. Lett.* **26**, 373 (2001).
  51. B. Schenkel, J. Biegert, U. Keller, C. Vozzi, M. Nisoli, G. Sansone, S. Stagira, S. De Silvestri, and O. Svelto, *Opt. Lett.* **28**, 1987 (2003).
  52. G. G. Paulus, F. Grabson, H. Walther, P. Villoresi, M. Nisoli, S. Stagira, E. Priori, and S. De Silvestri, *Nature* **414**, 182 (2001).
  53. A. Baltuska, T. Udem, M. Uiberacker, M. Hentschel, E. Goulielmakis, C. Gohle, R. Holzwarth, V. S. Yakovlev, A. Scrinzi, T. W. Hänsch, and F. Krausz, *Nature* **421**, 611 (2003).
  54. M. Hentschel, R. Kienberger, C. Spielmann, G. A. Reider, N. Milosevic, T. Brabec, P. Corkum, U. Heinzmann, M. Drescher, and F. Krausz, *Nature* **414**, 509 (2001).
  55. S.T. Cundiff and J. Ye, *Rev. Mod. Phys.* **75**, 325 (2003).
  56. A. Baltuska, T. Fuji and T. Kobayashi, *Phys. Rev. Lett.* **88**, 133901 (2002).
  57. S. Adachi, P. Kumbhakar, and T. Kobayashi, *Opt. Lett.* **29**, 1150 (2004).
  58. X. Fang and T. Kobayashi, *Opt. Lett.* **29**, 1282 (2004).
  59. M. Kakehata, H. Takada, Y. Kobayashi, K. Torizuka, Y. Fujihara, T. Homma, and H. Takahashi, *Opt. Lett.* **26**, 1436 (2001).

- 
60. C. Manzoni, G. Cerullo, and S. De Silvestri, *Opt. Lett.* **29**, 2668 (2004).
61. T. Fuji, A. Apolonski, and F. Krausz, *Opt. Lett.* **29**, 632 (2004).
62. C. Manzoni, C. Vozzi, E. Benedetti, G. Sansone, S. Stagira, O. Svelto, S. De Silvestri, M. Nisoli, and G. Cerullo, *Opt. Lett.* **31**, 963 (2006).
63. T. Fuji, N. Ishii, C. Y. Teisset, X. Gu, T. Metzger, A. Baltuska, N. Forget, D. Kaplan, A. Galvanauskas, and F. Krausz, *Opt. Lett.* **31**, 1103 (2006).
64. C. Vozzi, G. Cirimi, C. Manzoni, E. Benedetti, F. Calegari, G. Sansone, S. Stagira, O. Svelto, S. De Silvestri, M. Nisoli, and G. Cerullo, *Opt. Expr.*, in press (2006).
65. M. D. Perry, D. Pennington, B. C. Stuart, G. Tietbohl, J. A. Britten, C. Brown, S. Herman, B. Golick, M. Kartz, J. Miller, H. T. Powell, M. Vergino, and V. Yanovsky, *Opt. Lett.* **24**, 160 (1999).
66. A. Dubietis, G. Jonusauskas, and A. Piskarskas, *Opt. Commun.* **88**, 437 (1992).
67. I.N. Ross, P. Matousek, M. Towrie, A.J. Langley, and J.L. Collier, *Opt. Commun.* **144**, 125 (1997).
68. J. Collier, C. Hernandez-Gomez, I.N. Ross, P. Matousek, C.N. Danson, and J. Walczak, *Appl. Opt.* **38**, 7486 (1999).
69. I.N. Ross, J. Collier, P. Matousek, C.N. Danson, N. Neely, R.M. Allott, D.A. Pepler, C. Hernandez-Gomez, and K. Osvay, *Appl. Opt.* **39**, 2422 (2000).
70. X. Yang, Z. Xu, Y. Leng, H. Lu, L. Lin, Z. Zhang, R. Li, W. Zhang, D. Yin, and B. Tang, *Opt. Lett.* **27**, 1135 (2002).
71. N. Ishii, L. Turi, V. S. Yakovlev, T. Fuji, F. Krausz, A. Baltuska, R. Butkus, G. Veitas, V. Smilgevicius, R. Danielius, and A. Piskarskas, *Opt. Lett.* **30**, 567 (2005).
72. C. P. Hauri, P. Schlup, G. Arisholm, J. Biegert, and U. Keller, *Opt. Lett.* **29**, 1369 (2004).
73. R. Th. Zinkstok, S. Witte, W. Hogervosrt, and K.S.E. Eikema, *Opt. Lett.* **30**, 78 (2005).
74. P. Matousek, B. Rus, and I.N. Ross, *IEEE J. Quantum Electron.* **36**, 158 (2000).